Combustion and Flame 193 (2018) 502–519

Contents lists available at ScienceDirect

Combustion and Flame

journal homepage: www.elsevier.com/locate/combustflame

A physics-based approach to modeling real-fuel combustion chemistry - I. Evidence from experiments, and thermodynamic, chemical kinetic and statistical considerations

Hai Wang[a,*], Rui Xu[a], Kun Wang[a], Craig T. Bowman[a], Ronald K. Hanson[a], David F. Davidson[a], Kenneth Brezinsky[b], Fokion N. Egolfopoulos[c]

[a] Department of Mechanical Engineering, Stanford University, Stanford, CA 94305-3032, USA
[b] Department of Mechanical and Industrial Engineering, University of Illinois at Chicago, Chicago, IL 60607, USA
[c] Department of Aerospace and Mechanical Engineering, University of Southern California, Los Angeles, CA 90089-1453, USA

ARTICLE INFO

Article history:
Received 21 November 2017
Revised 12 March 2018
Accepted 14 March 2018
Available online 21 April 2018

Keywords:
Kinetics
Aviation fuel
Reaction model
HyChem

ABSTRACT

Real distillate fuels usually contain thousands of hydrocarbon components. Over a wide range of combustion conditions, large hydrocarbon molecules undergo thermal decomposition to form a small set of low molecular weight fragments. In the case of conventional petroleum-derived fuels, the composition variation of the decomposition products is washed out due to the principle of large component number in real, multicomponent fuels. From a joint consideration of elemental conservation, thermodynamics and chemical kinetics, it is shown that the composition of the thermal decomposition products is a weak function of the thermodynamic condition, the fuel-oxidizer ratio and the fuel composition within the range of temperatures of relevance to flames and high temperature ignition. Based on these findings, we explore a hybrid chemistry (HyChem) approach to modeling the high-temperature oxidation of real, distillate fuels. In this approach, the kinetics of thermal and oxidative pyrolysis of the fuel is modeled using lumped kinetic parameters derived from experiments, while the oxidation of the pyrolysis fragments is described by a detailed reaction model. Sample model results are provided to support the HyChem approach.

1. Introduction

Chemical reaction modeling of combustion processes requires a set of pre-specified thermodynamic conditions as the initial or boundary conditions. These conditions include the temperature and pressure, and the chemical identity of the reactant molecules and their initial concentrations. Conventional, petroleum-derived gasoline, aviation jet fuels, rocket fuels and diesel fuels have compositions that are not precisely defined, at least not to the level that can be treated by detailed chemistry modeling using the fuel composition as a part of thermodynamic input. These distillate fuels are usually comprised of hydrocarbons ranging in carbon numbers from 4 to 12, 7 to 18, and 8 to 20 for gasoline, jet and diesel fuels, respectively (e.g., [1–3]). Major classes of hydrocarbon compounds found in these fuels include normal paraffins, *iso*-paraffins, cycloparaffins, alkenes and aromatics. As an example, Fig. 1 presents typical compositions of three jet fuels.

Compositional complexities in real fuels usually preclude the possibility of identifying explicitly the molecular structure and concentration of every fuel constituent. For modeling their combustion behaviors, the principal approach adopted over the last decade is the surrogate-fuel approach (e.g., [5–14]). This approach attempts to mimic real-fuel combustion behaviors using a surrogate fuel comprised of several neat compounds of well-defined structure and composition to represent the chemical functionalities of a real fuel. A key advantage of the surrogate-fuel approach is that it removes the difficulty associated with the inability to define the composition of a fuel, thus transforming it into a problem that can be tackled, at least in principle, from fundamental reaction mechanisms and rates. There are, however, some drawbacks to the surrogate approach.

First, while the development of detailed reaction models of individual surrogate components can be carried out, building a surrogate mixture to mimic a real fuel is empirical. Matching the physicochemical properties (e.g., H/C ratio, average molecular weight, smoke point, and cetane number) does not necessarily yield a surrogate that accurately duplicates the combustion behavior of the real fuel. Only a careful selection of surrogate

* Corresponding author.
E-mail address: haiwang@stanford.edu (H. Wang).

https://doi.org/10.1016/j.combustflame.2018.03.019
0010-2180/

List of Symbols

A	Arrhenius prefactor
a	A stoichiometric coefficient in treating n-hexane pyrolysis
$($	Stoichiometric coefficient in HyChem formulation, yield of H atom per fuel "molecule" from the thermal decomposition of the fuel "molecule"
B	"Activation energy" in modified Arrhenius equation
b_a	A dependent stoichiometric variable in HyChem formulation
b_d	A dependent stoichiometric variable in HyChem formulation
β	Stoichiometric coefficient in HyChem formulation, yield of H atom per fuel "molecule" from the β-scission the fuel "radical" upon H-abstraction
c_p	Specific heat
e_a	A dependent stoichiometric variable in HyChem formulation
e_d	A dependent stoichiometric variable in HyChem formulation
ϕ	Equivalence ratio of fuel–air mixture
G^o	Standard Gibbs energy
γ	Stoichiometric coefficient in HyChem formulation, yield of methane per fuel "molecule" (inaddition to H-abstraction by the methyl radical)
H/C	Hydrogen-to-carbon ratio
H^o	Standard enthapy
H_v	Enthalpy of evaporation
$h^\circ_{f,298K}$	Standard-state enthalpy of formation
I/I_0	Ratio of transmitted-to-incident light intensities
K_{ext}	Counterflow flame extinction strain rate
k	Rate coefficient
L	Optical path length
LHV	Lower heating value
λ	Wavelength
λ_3	Stoichiometric coefficient in HyChem formulation, ratio of propene-to-ethylene yields
λ_4	Stoichiometric coefficient in HyChem formulation, ratio of butene-to-ethylene yields
$\lambda_{4,1}$	Stoichiometric coefficient in HyChem formulation, ratio of 1-butene-to-ethylene yields
$\lambda_{4,i}$	Stoichiometric coefficient in HyChem formulation, ratio of i-butene-to-ethylene yields
MW	Molecular weight
N	Absorbent number density
n_h	Number of hydrocarbon components in Monte Carlo simulations
n	Temperature exponent in modified Arrhenius equation
p	Pressure
p_5	Pressure behind reflected shock wave
σ_λ	Absorption cross section at wavelength λ
S^o	Standard entropy
S°_u	Laminar flame speed
$S_{u,\mathrm{ref}}$	Reference velocity in laminar flame speed measurement
s^o	Molar specific, standard entropy
σ	Standard deviation
T	Temperature
τ_{ign}	Shock-tube ignition delay
T_u	Unburned gas temperature
T_5	Temperature behind reflected shock wave
t	Reaction time
χ	Stoichiometric coefficient in HyChem formulation, yield of benzene to the total yield of benzene and toluene

components and tuning of the surrogate mixture composition based on actual measured real-fuel combustion properties would recover the kinetic behavior over the range of conditions tested with real fuels. Since the condition space is usually large for practical combustors, experimental measurements must be extensive and are time consuming. Then, having tested the combustion behaviors of the real fuel over the range of relevant conditions, the need for the surrogate would itself diminish, since the combustion properties of the real fuel would have been known or acquired from the experiments. Second, typical surrogates are composed of four or five neat compounds (e.g., [10,12]). Usually, detailed reaction models are developed and tested against experiments for single-component fuels. Kinetic coupling of the fragments of fuel components may occur in some combustion reaction processes. Hence, surrogate reaction models assembled by combining submodels of single-component hydrocarbons may have to be tested for this coupling. To fully verify the model accuracy, a wide range of experiments and validation tests are again needed in order to explore kinetic coupling of surrogate constituents on an exhaustive, combinatorial basis. Third, developing detailed reaction models for large hydrocarbons is by no means as fundamental as one would hope. The number of reactions could reach several thousands for a single hydrocarbon. It is daunting, if not impossible, to treat the great many reaction pathways and rate parameters by first-principles or experimentation.

The three considerations discussed above suggest that the surrogate approach is overall an empirical approach. It is also inefficient, if not impossible, to capture the combustion chemistry of real fuels over a wide range of thermodynamic condition space. Even more importantly, jet and diesel fuels are usually injected into an engine as a spray. The breakup and evaporation of the spray is critical to the subsequent combustion process. To this end, it is impossible to develop a four- or five-component surrogate that can match the distillation curve closely and produce a fuel vapor mixture that matches the chemical properties of a real fuel. If, for example, the lowest boiling-point hydrocarbon in the surrogate mixture belongs to a particular class of hydrocarbon compounds (e.g., an n-alkane), the ignition behavior of the surrogate would be sensitive only to that class of compounds as the fuel starts to evaporate. Yet, the distribution of the evaporated compounds toward the low-temperature part of the distillation curve are in fact similar to the distribution of the hydrocarbon compound classes of the entire distillate fuel, as demonstrated by Bruno and coworkers [15].

The current study seeks to advance an alternative concept. The approach, called HyChem (Hybrid Chemistry), employs a physics-based understanding of the primary reaction pathways in fuel combustion. It combines an experimentally constrained fuel-pyrolysis model with a detailed, foundational chemistry model for the oxidation of pyrolysis products to describe and predict the combustion behaviors of real, multi-component fuels. Historically, ideas and elements of the HyChem approach have existed for some time. For example, lumped reaction models have been used in fuel combustion and chemical process research for a long time (see, for example, the pioneering work of Ranzi [16]). Williams and coworkers have advocated a "simplified" reaction modeling approach for some time now and demonstrated such an approach to modeling JP-10 combustion [17,18]. In the current paper, we provide experimental evidence as well as thermodynamic, chemical kinetic and statistical justifications to support the HyChem approach. We also

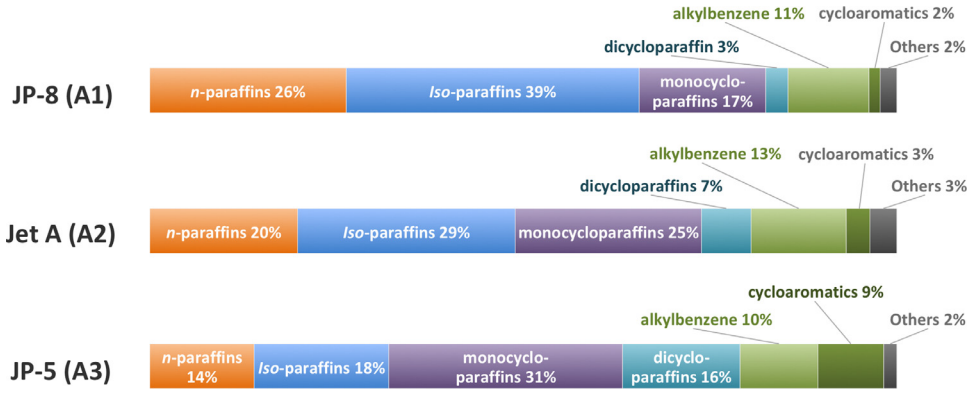

Fig. 1. Compositions of typical JP-8 (POSF10264), Jet A (POSF10325), and JP-5 (POSF10289) fuels [4]. Cycloaromatics refer to multi-ring compounds that contain at least one aromatic ring. (The POSF number bears no particular significance other than a batch number in the fuel repository where the fuel was acquired).

present a sample HyChem reaction model for a typical Jet A fuel (POSF10325) to illustrate its ability to predict the real-fuel combustion behavior. The discussion of the current paper focuses on high-temperature chemistry only. In the follow-up paper [19], we will present HyChem models for three jet fuels and two rocket fuels, including a discussion about the feasibility of treating the low-temperature chemistry in the negative temperature coefficient (NTC) region.

2. Simulation methods

Two modeling approaches were taken in the present work. The first one is a Monte Carlo simulation of the multi-component effect on the combustion properties of fuel mixtures using JetSurF 1.0 [20] and 2.0 [21] that were expanded to include reactions of aromatics, including ethyl-, *n*-propyl-, and *n*–butyl–benzene compounds and highly branched *iso*-paraffinic hydrocarbons, including neohexane and 2,2,4-trimethylpentane. The JetSurF model considers the high-temperature combustion chemistry of *n*-paraffinic compounds up to *n*-dodecane and alkylcyclohexane up to *n*-butylcyclohexane. The alkylated benzene and *iso*-paraffin submodels are based on the work of Lawrence Livermore Research Lab and National University of Ireland Galway [22–25]. This combined model is comprised of 421 species and 2616 reactions.

In the second approach, real-fuel combustion chemistry is explored using the HyChem approach, in which the kinetics of thermal and oxidative pyrolysis of the fuel is modeled using lumped kinetic parameters derived from experiments, while the oxidation of the pyrolysis fragments is described by a detailed reaction model. Key assumptions of the HyChem modeling approach, along with sample experimental and model test results that support the approach, are provided in Section 6. Details of the model and comparison of model predictions with a broad range of experimental data are found in the companion paper [19].

Solutions of the initial and boundary value problems were carried out using the ChemKin package [26]. Laminar flame structure was obtained from PREMIX [27] calculations employing multi-component transport and thermal diffusion. Non-premixed flame extinction strain rates were computed using a modified version [28] of an opposed-jet flow code [29] using a two-point continuation method [30]. Ignition delay is defined as the time to reach the maximum rate of OH* production under the adiabatic and constant volume condition. The computation for shock-tube pyrolysis was made following an adiabatic, constant-pressure assumption. Flow reactor simulation used the constant-temperature, constant-pressure assumption.

3. Experimental methods

3.1. Flow reactor facility

A flow reactor facility was used to investigate the oxidative pyrolysis kinetics of Jet A. The flow reactor is comprised of a vertical quartz reactor tube enclosed in a pressure vessel; detailed descriptions are provided in a recent study [31]. A liquid fuel was injected into a vaporizer by a syringe pump before being introduced into the reactor in a nitrogen carrier gas. The reaction products sampled by a cooled probe were sent to a 4-column micro gas chromatograph (Inficon microGC 3000) that provides real time detection. A non-dispersive infrared analyzer (NDIR) and a paramagnetic analyzer (PMA) were used for real-time measurements of CO, CO_2 and O_2. The total uncertainty in species concentration is ± 2–5% for most species.

3.2. Shock tube facilities

Pyrolysis speciation and ignition delay time (τ_{ign}) experiments were performed using both high- and low-pressure shock tubes. Descriptions of these two facilities are provided in a recent study [32]. Three diagnostic methods were used: pyrolysis speciation measurements via laser absorption, and τ_{ign} measurements via OH* emission and sidewall pressure. Laser absorption measurements took advantage of the Beer-Lambert law, i.e. $-ln[(I/I_0)_\lambda] = \sigma_\lambda NL$, to relate the measured absorbance $-ln[(I/I_0)_\lambda]$, with N the absorbent number density and L the optical path length, to the unknown species mole fraction X, using measured absorption cross sections σ_λ. In the C_2H_4 and CH_4 time-history measurements, where one product dominated the absorbance at a particular wavelength and other species have nearly constant absorbance at this wavelength, a two-wavelength differential method was used to determine the concentration of the dominant absorber [33].

Experimentally determined τ_{ign} values in this study are defined as the time interval from the passage of the reflected shock wave across the observation port to the time of the measured onset of pressure rise or OH* emission. For the experiments conducted herein, the two measurements yield results that are well within their respective experimental uncertainties. This onset is determined by back extrapolating the rapidly rising pressure or emission signal to the intersection with the pre-rise baseline value.

3.3. Laminar flame speeds and extinction strain rates

Laminar flame speeds, S_u°, were measured in the counterflow configuration for a wide range of equivalence ratios at atmospheric

pressure and an unburned mixture temperature $T_u = 403$ K. The liquid fuel system consists of a high-pressure precision pump that supplies fuel to a quartz nebulizer and is sprayed into preheated stream of air. A double pulsed ND:YAG laser and a high performance 12 bit CCD camera with 1376×1040 pixels of resolution was used to acquire Particle Image Velocimetry (PIV) images. The minimum axial velocity along the system centerline just upstream of the flame was defined as a reference flame speed, $S_{u,\mathrm{ref}}$, and the maximum absolute value of axial velocity gradient is defined as a local strain rate, which is varied and its effect on $S_{u,\mathrm{ref}}$ is recorded. S_u° was determined through computationally-assisted extrapolation to zero stretch [34]. The $2\int$ standard deviations in S_u° are indicated with uncertainty bars in relevant figures.

Extinction strain rates, K_{ext}, were measured also in the counterflow configuration at atmospheric pressure for non-premixed flames by impinging a fuel/N_2 stream at $T_u = 473$ K onto an ambient temperature O_2 stream. The strain rate K was measured on the fuel side and extinction was achieved by reducing slightly the fuel concentration.

4. Fuel decomposition first followed by oxidation

4.1. Flame structure and species time histories during high-temperature oxidation of single-component fuels

In a high-temperature combustion process, large fuel molecules first undergo decomposition into several small pyrolysis fragments, followed by the oxidation of these fragments to produce final combustion products. This generally is true regardless of whether or not molecular oxygen is present in the system. To illustrate this point, Fig. 2 depicts the calculated structure of an adiabatic laminar premixed flame of *n*-butylcyclohexane in air. The computation was carried out using JetSurF 2.0 at 1 atm pressure, 298 K unburned temperature and 1.2 equivalence ratio. As seen, the fuel decomposes into several small species long before the flame (marked by the peak concentration of the electronically excited CH radical). The concentrations of the pyrolysis products peak in the preheat region. For *n*-butylcyclohexane, key pyrolysis intermediates are C_2H_4, H_2, CH_4 and C_3H_6, all of which have substantially larger molecular diffusivities than the parent fuel. They enter into the flame by diffusion (along with O_2) and are oxidized leading to CO, H_2O and CO_2 production and heat release. The decay of the O_2 concentration in the pyrolysis zone is due to molecular diffusion and has almost nothing to do with its consumption by chemical reactions.

The flame structure just discussed is typical for large hydrocarbon fuels, as discussed by Peters some time ago [35]. There are two principal reasons leading to the observed flame structure. Because of the disparity in the molecular diffusivities of the fuel and oxygen, without fragmenting the fuel molecule, the large Lewis number of the mixture would essentially render the flame unstable [36,37]. For such a flame to be stable, then, the second reason must be the ease with which the fuel undergoes decomposition in the preheat zone, in which the temperature is high enough and small radical species (e.g., H and OH) are relatively abundant due to diffusion. These species interact with the fuel molecule and facilitate its dissociation in the preheat zone of the flame.

The pyrolysis zone in flames has a convective residence time of O (10^2 μs) and the temperature ranges roughly from 1100 to 1450 K. These are the conditions applicable for the thermal decomposition of a wide range of hydrocarbon fuels. To further illustrate and expand on the above point, the time histories of key species during *n*-heptane oxidation behind a reflected shock at the initial temperature of 1365 K are shown in Fig. 3. This temperature (i.e., 1365 K) is close to the upper end of the temperature window of fuel decomposition in typical flames; the experimental data were

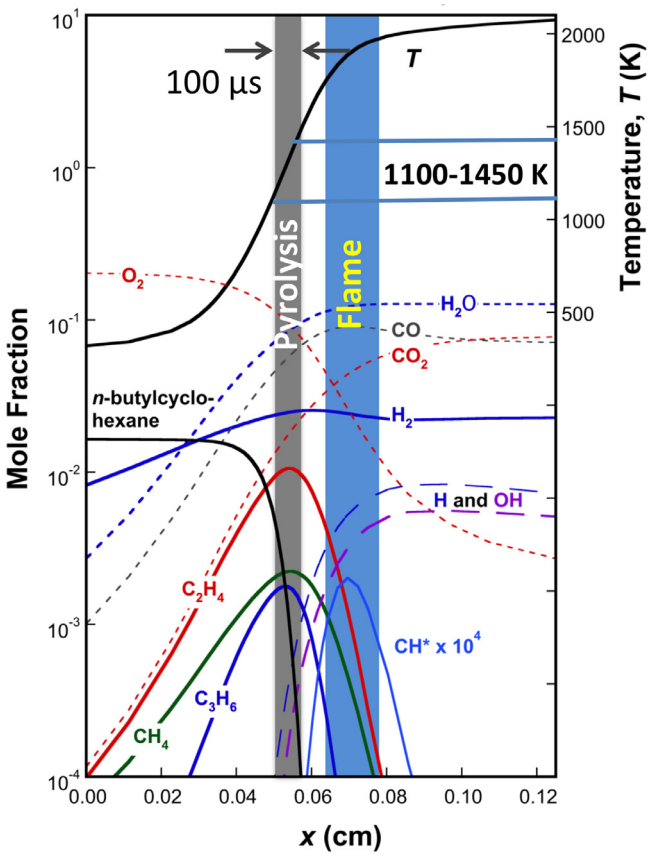

Fig. 2. Structure of an adiabatic one-dimensional, premixed, *n*-butylcyclohexane-air flame with an unburned temperature of 298 K, 1 atm pressure and 1.2 equivalence ratio, computed using JetSurF 2.0 [21].

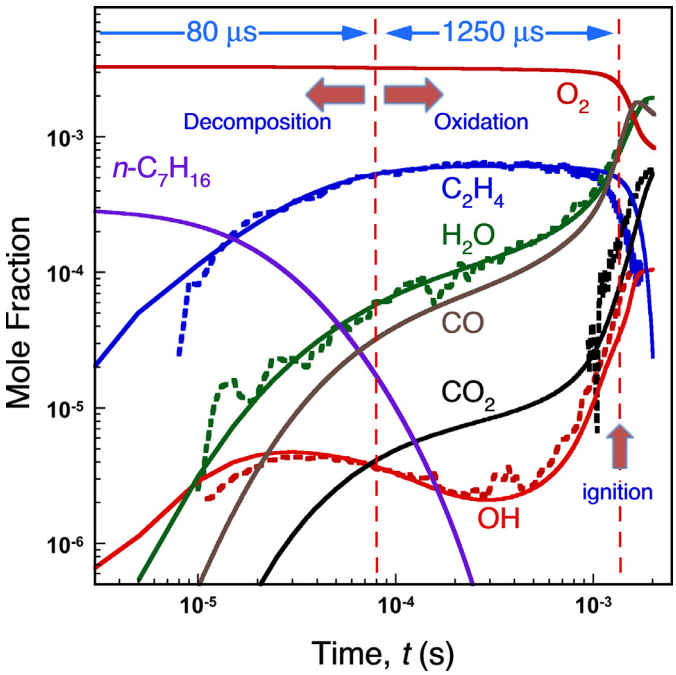

Fig. 3. Key species time histories of *n*-heptane oxidation in a shock tube (300 ppm n-C_7H_{16}/3300 ppm O_2/Ar, $T_5 = 1365$ K, $p_5 = 2.35$ atm). Dashed lines: experimental data [38]; lines: simulation using an optimized JetSurF 1.0 [39]. The line dividing decomposition and oxidation is set at an arbitrary value of 95% fuel disappearance.

taken from Davidson et al. [38] and the computed results are from Sheen and Wang [39]. Unlike flames in which the fuel decomposition is facilitated by free radicals diffused from the flame, fuel oxidation in the shock tube relies on free-radical build-up; and fuel decomposition that proceeds the oxidation requires a somewhat longer reaction time at comparable temperatures. Nevertheless, over the ~1 ms induction time leading to ignition, the conversion of the fuel to C_2H_4 (and a handful of other pyrolysis products not shown) through thermal decomposition is nearly complete by 80 μs. During this period and extending to around 1000 μs, there is very little O_2 consumption or CO_2 production. In other words, the fuel decomposes to C_2H_4 and other intermediates without consuming O_2 appreciably.

Clearly, the thermal decomposition of the fuel is fast and the oxidation of the decomposed products is rate limiting during the entire course of reaction leading to ignition. Similarly, the thermal decomposition of the fuel molecule in flames is fast within the flame time scale, and the oxidation of the decomposed products leading to heat release occurs at a higher temperature. Hence, the fragment oxidation process is again rate limiting. The same behavior has been observed in several other studies. For example, Malewicki and Brezinsky [40] determined that over the temperature range of 940–1600 K the decomposition of *n*-decane precedes O_2 disappearance and is insensitive to the initial O_2 concentration or the equivalence ratio ranging from 0.5 to infinity. Davidson et al. [41,42] presented similar evidence in their experiments on *n*-dodecane and *n*-hexadecane.

4.2. Key intermediates: thermodynamic and chemical kinetic considerations

The discussion above reveals two general rules in high-temperature oxidation of large hydrocarbon molecules:

- Fuel molecules undergo thermal or oxidative thermal decomposition followed by oxidation of decomposed products. The two processes are separable in time or spatial scales.
- The number of significant products or intermediates is small, or six to ten in all. It is the composition of these thermal decomposition products that determines the combustion properties of the original, multi-component real fuels.

In what follows, we make relevant chemical kinetic modeling observations and present thermodynamic arguments that support the two rules just stated.

Figure 4 shows the time histories of temperature and key species computed for the isobaric decomposition of 1.13% (mol) *n*-dodecane in N_2 at 10 bar pressure and an initial temperature of 1300 K. The left panel gives results under the adiabatic condition; the right panel presents the profiles for an isothermal condition. JetSurF 1.0 [20] was used for the simulation. The equilibrium species concentrations are shown in the respective grey, shaded areas.

Several observations can be made. Due to reaction endothermicity, the adiabatic pyrolysis temperature drops by more than 100 K for the initial *n*-dodecane concentration calculated. For the initial temperature computed, the dominant product of decomposition is C_2H_4 for reaction time as long as 100 ms. Beyond this reaction time, the distribution of the reaction products slowly approaches that of the equilibrium condition, where temperature rises somewhat due to the exothermicity associated with aromatics production from C_2H_4 and other small species. The product distributions and time histories are similar between the isothermal and adiabatic runs, except the isothermal case is slightly faster because of a higher (constant) temperature. Over the flame-relevant time scales, the dominant products of decomposition are very few. These key products are C_2H_4, H_2, CH_4, C_3H_6, 1-C_4H_8, 1,3-C_4H_6 and C_2H_2.

The group of pyrolysis intermediates reaches a plateau in their yields within 100 μs for the condition tested, and their concentrations remain at these levels for a substantially longer period of time. This can be seen in Fig. 5, which is a zoomed-in view of the right panel of Fig. 4. For the temperature considered, the number of species is small and the structure of the key species around the time window is rather simple. The species concentrations reach their plateau values or a quasi-equilibrium state by about 100 μs. As the chain reaction carrier, the concentration of radical species is rather low over that period of time; see, for example, the methyl radical curve of Fig. 5.

The dominance of C_2H_4 as an intermediate of hydrocarbon pyrolysis has been known for a long time (see, e.g., [43]). The cause is largely thermodynamic and chemical kinetic in nature. The decomposition of a majority of hydrocarbon compounds found in real liquid fuel is endothermic; and the driving force for decomposition is the entropy increase. Figure 6 shows the various chemical equilibrium states from a hypothetical fuel mixture with an average molecular formula of $C_{11}H_{22}$ at an initial mole fraction of 1.13%, under the constant temperature (1300 K) and pressure (10 bar). This concentration represents a fuel–air mixture with 6% (wt) of the Jet A fuel but with the air O_2 replaced by N_2 in the mixture. The temperature used in the calculation is near the mid-range of the fuel decomposition window in a typical flame (*cf*, Fig. 2). The thermochemical data were taken from earlier work [21,44].

The equilibrium composition of a given state was determined by removing the most dominant, higher-molecular weight compound(s) to the right of that state from the calculation. For example, removing graphite, C(S), from the list of equilibrium species considered has the effect of creating an infinitely large kinetic energy barrier to the formation of graphite. For this situation and the species considered in the equilibrium calculation (with polycyclic aromatic hydrocarbons up to the size of pyrene), pyrene becomes the most dominant equilibrium product in carbon mass (state 5). Overall, fuel decomposition is largely driven by an increase in system entropy leading to a decrease in the Gibbs free energy. At the same time, the endothermicity of thermal decomposition increases the system enthalpy, at least initially. Overall, the Gibbs free energy decreases as the entropy-driven decomposition proceeds, from the fuel to the most favored thermodynamic state to the right.

The final thermodynamic equilibrium state (state 6) for the thermal decomposition of $C_{11}H_{22}$ is dominated by solid carbon and hydrogen. For such an endothermic process, the driving force of pyrolysis is the entropy increase due to the release of ~11 moles of H_2 per mole of $C_{11}H_{22}$ consumed. Repeating the procedure of removing dominant, higher-molecular weight compounds from pyrene to all aromatics, the equilibrium system reaches an island of small species that contain mainly $C_{2\text{-}4}$ alkyne and alkene, CH_4 and H_2. All of these thermodynamic states are associated with endothermic reaction processes. As soon as C_2H_2 is removed from equilibrium calculation (from state 3 to state 2), C_2H_4 becomes one of the dominant product species. Kinetically, the enthalpy barrier from State 1 to 3 would impede the progress to an extent, as these processes are all endothermic. More importantly, C_2H_4 resists further decomposition below around 1400 K, owing to its large C–H bond energy. The half life of ethylene due to its thermal decomposition is of the order of 10^1–10^2 ms at 1300 K over the pressure range of 1–100 atm (see Fig. S1 of the Supplementary Materials), which is much longer than the typical residence time of the pyrolysis zone in a flame or the induction time leading to high-temperature homogeneous ignition.

Beyond thermodynamics, three kinetic and mechanistic principles are worth considering. We illustrate the first principle using *n*-hexane pyrolysis as an example. From a consideration of reac-

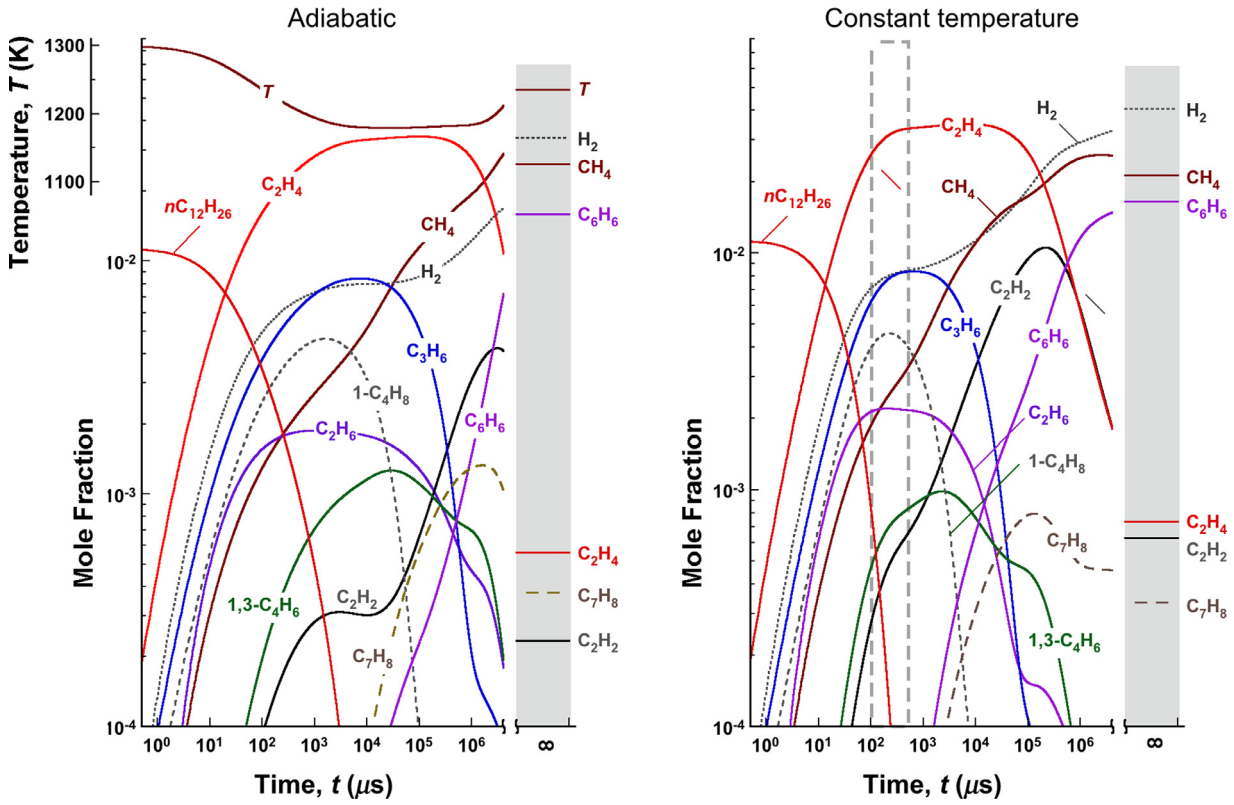

Fig. 4. Time histories of temperature and key species computed for isobaric thermal decomposition of 1.13% (mol) *n*-dodecane in N_2 at 10 bar pressure and an initial temperature of 1300 K, under the adiabatic (left panel) and constant-temperature (right panel) conditions. Shaded areas: product distributions of chemical equilibrium without considering the formation of aromatic compounds beyond toluene and solid carbon. The shaded area in the right panel has the composition identical to that of state 4 in Fig. 6. The time scale of fuel thermal decomposition in typical laminar premixed flames is represented roughly by the rectangle marked by dashed lines in the right panel. The computations were carried out using JetSurF 1.0 [20].

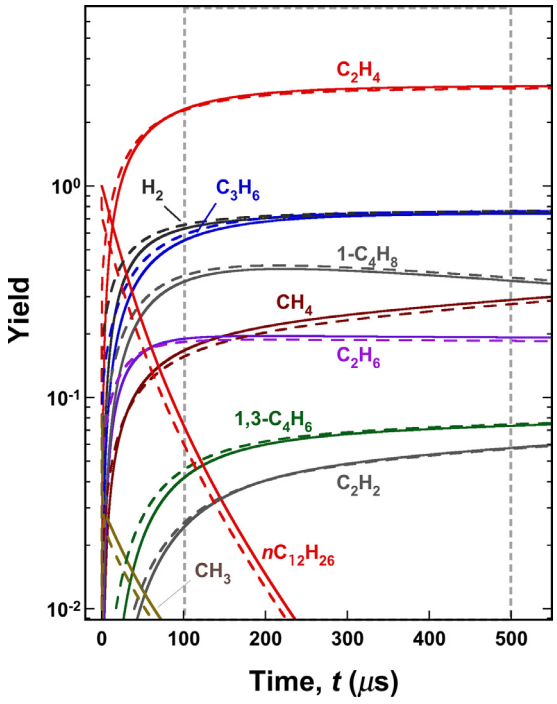

Fig. 5. Zoomed in view of the right panel of Fig. 4, showing the time histories of the parent *n*-dodecane and yields of the decomposed species over the time scale relevant to typical laminar premixed flames. Solid lines: 1.13% (mol) *n*-dodecane in N_2; dashed lines: with 0.1% (mol) H, 0.1% (mol) OH and 0.01% (mol) O added to the initial mixture.

tion rates and supported by the results of detailed modeling (e.g., [45]), several observations can be made:

(1) The H-abstraction produces one primary or either of two secondary hexyl radicals, as shown in Fig. 7. The energy barriers to H-shift isomerization reactions among these hexyl radicals are all small. They are ~15 kcal/mol for 1,5- and 1,6-H shift isomerization and ~22 kcal/mol the 1,4 H-shift (see, e.g., [46]). The corresponding isomerization time scale is < 1 μs above 1000 K.

(2) The C–C β-scission reactions of the three alkyl radicals are also fast. The maximum energy barrier of these reactions is 35 kcal/mol (see, e.g., [47]). Using an A factor value of $\sim 5 \times 10^{13}$ s^{-1}, we find that at $T > 1000$ K the half life of these radicals is 1 μs or shorter, and as such their dissociation is also almost instantaneous on the time scale relevant to any combustion process.

(3) In contrast, C–H β-scission reactions are substantially slower than C–C β-scission because of the stronger bond strengths, by over 10 kcal/mol. They are essentially negligible. The only exception is the C_2H_5 (ethyl) radical since it does not have a β C–C bond. It undergoes H elimination to produce $C_2H_4 + H$ (the actual time scale is 5–18 μs for pressures ranging from 100 to 1 bar at 1000 K, and < 1 μs at 1200 K and above).

(4) The products of the C–C β-scission are also presented in Fig. 7. They are C_2H_4, C_3H_6, 1-C_4H_8, 1-C_5H_{10}, H, and CH_3. The CH_3 and H radicals generated from the decomposition process are consumed by H-abstraction of *n*-C_6H_{14}; and these are the sources of CH_4 and H_2. The C–C β-scission of the 3-hexyl radical (CH_3–CH_2–CH_2–•CH–CH_2–CH_3) yields 1-$C_4H_8 + C_2H_5$ or 1-C_5H_{10} (1-pentene) + CH_3. The branching

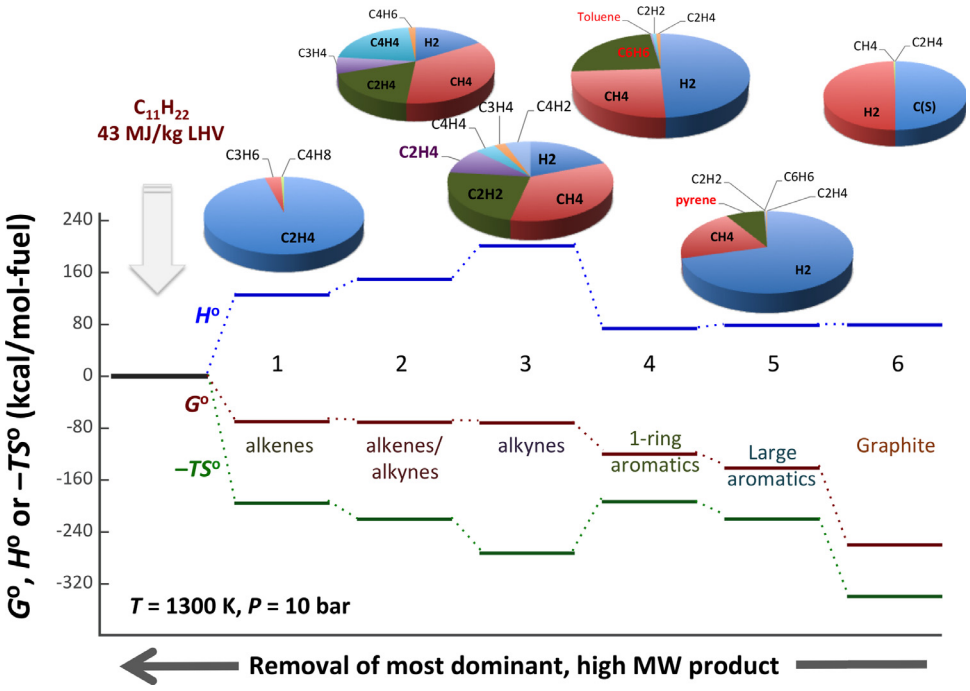

Fig. 6. Diagram of enthalpy and entropy contributions to the changes in the Gibbs free energy for an initial state corresponding to a hypothetical fuel compound or mixture (1.13% mol or 6% by mass) in N_2 at 1300 K and 10 bar. Properties of the fuel compound: $C_{11}H_{22}$ (a typical Jet-A or JP-8 fuel), lower heating value (LHV) = 42.8 MJ/kg, $s°(298K)$ = 129.5 cal/mol-K and c_p (J/mol-K) = 55.82 T^{*5} − 251.5 T^{*4} + 451.2 T^{*3} − 462.5 T^{*2} + 361.4 T^{*} − 20.0. The entropy and specific heat values are based on a three-component surrogate mixture comprised of 60% (mol) *n*-dodecane/20% (mol) *n*-butylcyclohexane/20% (mol) trimethylbenzene. The equilibrium composition of a given state was computed by removing the most dominant, high molecular weight compound(s) to the right of that state from the equilibrium calculation.

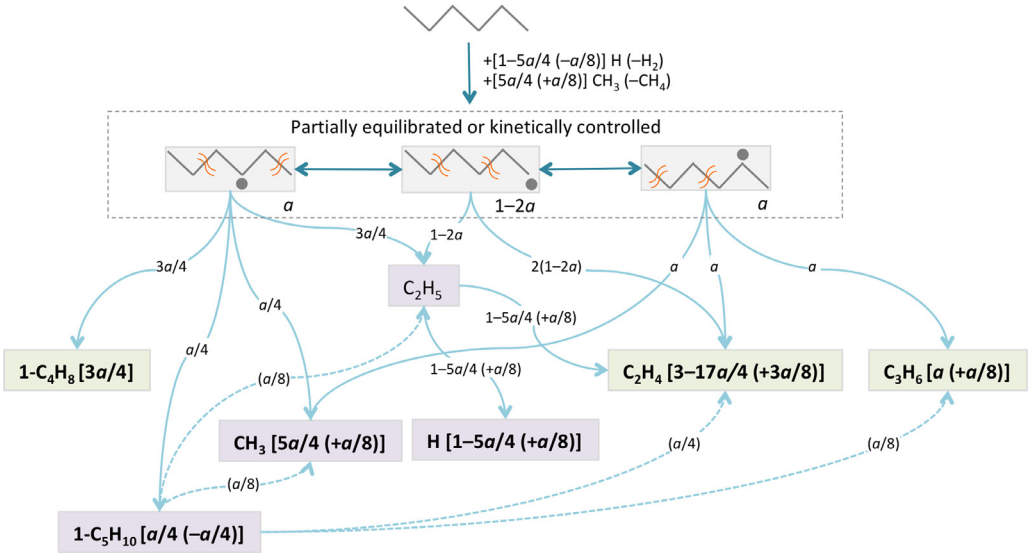

Fig. 7. Schematic illustration of the pathway and product branching ratio during the initial thermal decomposition of *n*-hexane.

ratio is almost independent of pressure above ~1 atm, but is weakly dependent on temperature. The rate ratio of the 1-C_4H_8 + C_2H_5 channel to the combined 1-C_4H_8 + C_2H_5 and 1-C_5H_{10} + CH_3 channels varies from around 0.8 at 1000 K to 0.6 at 1500 K. Here we assume that this branching ratio is a constant and equal to 3/4. The lifetimes of C_3H_6, 1-C_4H_8 and 1-C_5H_{10} are shorter than that of C_2H_4 (*cf*, Figs. S1-S3 of the Supplementary Materials). They could be converting to C_2H_4 and other products while *n*-hexane is consumed. The subsequent thermal decomposition of C_3H_6 and 1-C_4H_8 are not considered in Fig. 7. They can be treated by detailed modeling, as will be discussed later.

(5) The composition of the aforementioned products depends on the relative concentrations of the hexyl radicals. Since the H-shift isomerization in the hexyl radicals and the C–C β-scission are both facile, the composition of the hexyl radical isomers is both thermodynamically and kinetic controlled. We make two limiting treatments to show that they yield essentially the same results as far as the ability of the model (to be discussed) to predict key combustion properties of *n*-hexane is concerned. The first treatment is thermodynamic in nature; and it assumes that the hexyl radicals are in partial equilibrium among themselves. The second treatment is kinetic by assuming that their concentrations are kinetically controlled by the rates of the respec-

tive H-abstraction reactions. In both treatments, the two secondary hexyl radicals have roughly the same concentrations. In the equilibrium treatment, the equal concentration is the result of nearly identical thermochemical properties of the two secondary hexyl radicals, while in the kinetic treatment the rate constants of the H-abstraction reactions on the secondary H atoms in *n*-hexane are roughly equal. Let a be the yield or the mole of each of the secondary hexyl radicals per mole of *n*-hexane consumed. The yield of the primary radical is then 1–2a, as depicted in Fig. 7.

The observations made above allow us to treat the complex reaction pathways and rates in a simple manner. Without considering 1-C_5H_{10} decomposition (i.e., considering only the solid lines of Fig. 7), we may treat the reaction products from the decomposition of the three hexyl radicals by

$$[p\text{–}C_6H_{11}, s1\text{–}C_6H_{11}, s2\text{–}C_6H_{11}]_{eq} \rightarrow (3-17a/4)C_2H_4 + aC_3H_6 + (3a/4)1\text{–}C_4H_8 + (a/4)1\text{–}C_5H_{10} + (5a/4)CH_3 + (1-5a/4)H$$

Then, a quasi-steady state treatment for the hexyl radicals allows the overall reactions to be written in a lumped step as

$$n\text{–}C_6H_{12} + R \rightarrow RH + (3-17a/4)C_2H_4 + aC_3H_6 + (3a/4)1\text{–}C_4H_8 + (a/4)1\text{–}C_5H_{10} + (5a/4)CH_3 + (1-5a/4)H \quad (1)$$

where $R = H$ and CH_3 in a pyrolysis process. In an oxidative process, additional R species include O, OH, O_2, and HO_2.

The coefficient a in Eq. (1) is not a function of pressure or stoichiometry as its value is governed by the equilibrium constant of the H-shift isomerization of the hexyl radicals and by the rate coefficients of H-abstraction reactions. a can be a function of temperature in principle, but the actual dependence is weak. For *n*-hexane and using the thermochemical data of JetSurF 2.0 [21], $a = 0.46$ at 1000 K and 0.43 at 1500 K in the thermodynamic treatment. In the kinetic treatment and for $R = H$, the a values are 0.41 and 0.38 at 1000 and 1500 K, respectively. For $R = CH_3$, the respective a values are 0.43 and 0.41. The average a value is 0.44 in the thermodynamic treatment and 0.40 in the kinetic treatment. In other words, the two treatments produce only 10% difference in the concentrations of the second hexyl radicals, and thus minor differences in the distribution of the decomposition products shown in Fig. 7.

To test the accuracy of the simplified, analytic treatments, we compared decomposition species concentrations as predicted by Eq. (1) and detailed modeling. The rate constants of Eq. (1) are simply those of the respective H-abstraction reactions of H and CH_3 of the detailed model. Clearly, there is no reason to believe that these rate constants should be dependent of the pressure and composition. Figure S4 of the Supplementary Materials shows the time histories of key species during *n*-hexane thermal decomposition, comparing the results of detailed JetSurF 2.0 and the simplified model combining the analytic expression (1) using $a = 0.44$ (the thermodynamic treatment) with USC Mech II—the $H_2/CO/C_1\text{–}C_4$ submodel of JetSurF 2.0. Figure S5 presents the similar results for the kinetic treatment ($a = 0.40$). Except for the initial few microseconds, both simplified models capture the species concentration profiles from detailed modeling rather well. More importantly, the ignition delay times of *n*-hexane computed using the simplified models do not differ significantly from detailed modeling, as seen in Fig. S6. In general, the equilibrium treatment for the hexyl radicals produces results closer to those of the detailed reaction model than the kinetic treatment. The applicability of the above treatment and the generality of the five observations discussed earlier have been tested for four octane isomers, ranging from *n*-octane to the most branched 2,2,3,3-tetramethylbutane, all with success [48].

The key point of the above analysis is that the stoichiometric parameter a is independent of pressure or stoichiometry. It has a weak temperature dependency but can be treated as a constant. Since the stoichiometric coefficients in Eq. (1) depend on the a value only, they are also roughly constant with respect to changes in temperature, pressure and stoichiometry within the range of applicability of the model. The assumption produces a maximum error of ± 5% in the stoichiometric coefficients of Eq. (1).

It is possible to simplify Eq. (1) when the temperature is above 1200 K and/or radical species are abundant. Under these conditions, the lifetime of 1-C_5H_{10} is quite short, and as such it may be treated by instantaneous decomposition via two reactions of equal reaction rates:

$$1\text{-}C_5H_{10} + H \rightarrow 2C_2H_4 + CH_3$$

$$1\text{-}C_5H_{10} + H \rightarrow C_3H_6 + C_2H_5 \quad (5)$$

With the above treatment (following the dashed lines of Fig. 7), Eq. (1) becomes

$$n\text{–}C_6H_{12} + R \rightarrow RH + (3-31a/8)C_2H_4 + (9a/8)C_3H_6 + (3a/4)1\text{–}C_4H_8 + (11a/8)CH_3 + (1-11a/8)H \quad (2)$$

For Eq. (2), the temperature dependence of the branching ratio of 1-C_5H_{10} breakdown adds less than ± 1% error in the stoichiometric coefficients. The yields directly calculated from the stoichiometric coefficients are also presented in Figs. S4 and S5, comparing Eqs. (1) and (2). As seen, the results of the simplification are satisfactory.

The second kinetic and mechanistic issue is the variation of fuel reactant structure and its impact on the pyrolysis product distribution. For example, the aromatic compounds in real fuels are mostly alkylated benzene. Owing to the stability of the benzene ring, the thermal decomposition of alkyl benzene would include C_6H_6 (benzene) and C_7H_8 (toluene). Their formation is largely because of the stability of the phenyl and benzyl radicals. The likely fragments from the alkyl functional group(s) are again C_2H_4, CH_4, and C_3H_6. In some cases, xylene and trimethylbenzene isomers may form, depending on the nature of the alkylbenzene compounds found in the fuel. The naphthene compounds are probably dominated by alkylcyclohexane. As shown in Fig. 2, the thermal decomposition of *n*-butylcyclohexane is dominated also by the production of C_2H_4, CH_4, and C_3H_6. The last type of real-fuel constituents to consider is *iso*-paraffins. In general, *iso*-paraffins have high octane and low cetane numbers, as these numbers are related to the ease with which the ROO radical undergoes internal H abstraction, leading to R'OOH production. During thermal decomposition above 1000 K, *iso*-paraffins or *iso*-alkyl functional groups in aromatics and alkylcyclohexane compounds can produce a substantial amount of C_3H_6 and *i*-C_4H_8. They may be viewed as molecular analogs of C_2H_4 with one or both H atoms on a single carbon atom replaced by the CH_3 group. Altogether, the decomposition products to consider are C_2H_4, H_2, CH_4, C_3H_6, 1-C_4H_8 (1-butene), *i*-C_4H_8 (*iso*-butene), C_6H_6 (benzene) and C_7H_8 (toluene). Cyclopentadiene and 1,3-butadiene join this list in some cases, which will be discussed in a future publication.

The last kinetic issue concerns the presence of initial radicals (H, O, and OH). They speed up the dissociation of the fuel but hardly impact the pyrolytic product distribution. As shown in Fig. 5 by the dashed lines, the addition of 1000 ppm (mol) each of H and OH and 100 ppm (mol) of the O atom at time zero presents some impact on the decomposition rate of *n*-dodecane, but they hardly change the branching ratios of the products. In the presence of molecular oxygen, fuel thermal decomposition can become faster but the consumption of O_2 and the changes in the decomposition product distribution are both negligible.

Table 1
Fuel components and their properties.

No	Compound	Chemical formula	MW (kg/kmol)	$h^{\circ}_{f,298\,K}$ (kcal/mol)	LHV (MJ/kg)
Normal paraffins					
1	*n*-dodecane	*n*-$C_{12}H_{26}$	170.3	−69.7	44.5
2	*n*-decane	*n*-$C_{10}H_{22}$	142.3	−59.8	44.6
3	*n*-nonane	*n*-C_9H_{20}	128.3	−54.9	44.7
4	*n*-octane	*n*-C_8H_{18}	114.2	−50.0	44.8
5	*n*-heptane	*n*-C_7H_{16}	100.2	−45.1	44.9
Iso-paraffins					
6	neohexane	*neo*-C_6H_{14}	86.2	−45.2	44.8
7	2,2,4-trimethylpentane	*i*-C_8H_{18}	114.2	−53.4	44.7
Alkylcyclohexane compounds					
8	*n*-butylcyclohexane	*c*-C_6H_{11}-*n*-C_4H_9	140.3	−51.5	43.8
9	*n*-propylcyclohexane	*c*-C_6H_{11}-*n*-C_3H_7	126.2	−45.4	43.8
10	ethylcyclohexane	*c*-C_6H_{11}-C_2H_5	112.2	−40.4	43.8
11	methylcyclohexane	*c*-C_6H_{11}-CH_3	98.2	−35.9	43.8
12	cyclohexane	*c*-C_6H_{12}	84.2	−29.5	43.8
Alkylbenzene compounds					
13	*n*-butylbenzene	C_6H_5-*n*-C_4H_9	134.2	−2.9	41.8
14	*n*-propylbenzene	C_6H_5-*n*-C_3H_7	120.2	1.9	41.6
15	ethylbenzene	C_6H_5-C_2H_5	106.2	7.0	41.3
16	toluene	$C_6H_5CH_3$	92.1	12.0	40.9

5. Principle of large component number – multi-component real fuels are not more complex than neat fuels

The combustion chemistry of multi-component real fuels is historically considered more complex than that of a single-component fuel. Here, we examine the validity of this notion. For this purpose, Monte Carlo simulations were carried out for hydrocarbon fuel mixtures. The simulations reveal a central rule for real, multi-component fuel combustion and dispels the preconceived notion concerning the impact of the chemical complexity associated with multi-component real fuels on our understanding. That is, *when the number of components in a fuel mixture becomes large enough* (> 12–14)*, the rate behavior of the mixture exhibits diminishing sensitivity toward fuel composition regardless of what components are found in the mixture.* The rule is rooted in the fundamental statistical theory in a way similar to the law of large number [49], and explains very well the small sensitivity of air-breathing engine performance to fuel composition variations. Monte Carlo simulations with a significantly broadened scope are available in a separate study [50].

Table 1 lists 16 fuel components considered in the Monte Carlo simulations. The two *iso*-paraffinic compounds chosen here are those that represent the highly branched *iso*-alkanes. In petroleum-derived jet fuels, this type of compounds is probably not abundant, as will be discussed later. For our simulations, we selected n_h ($n_h = 2, 3, 4, \ldots, 16$) number of hydrocarbon components randomly from Table 1 to form hypothetical fuel mixtures with each component assigned with a randomly chosen mole fraction in the fuel mixture.

Figure 8 shows the distributions of ignition delay times computed for the Monte Carlo fuel samples, all in air at a fuel mass fraction of 6%, an initial temperature of 1300 K and 1 atm pressure. Clearly, as the number of components increases, the variation in τ_{ign} diminishes. For a 2-component mixture, τ_{ign} can vary by an order of magnitude, whereas the 16-component mixtures produce a variation in τ_{ign} around only 13% (2-standard deviation). In fact, the 2σ values asymptote to 13% when $n_h \geq 14$, which is probably smaller than the measurement uncertainty in most shock tube facilities. Taking ± 20% as the measurement uncertainty of the shock-tube ignition delay measurement, which corresponds to roughly ± 15 K uncertainty in temperature behind the reflected shock wave, the current analysis suggest that with 95% confidence, fuels with 12 or more arbitrary hydrocarbon components would yield statistically the same ignition delay times under the conditions tested, as long as the fuel composition is based on an unbiased, random sampling with respect to hydrocarbon classes. The above finding is supported by a recent shock-tube study of the ignition delay time for a variety of aviation and rocket fuels [32], all of which are distillate, multi-component fuels and have closely similar high-temperature ignition delay times under the conditions tested.

The results just discussed have several far-reaching implications. First, the combustion chemistry of multi-component fuels is not more complex to treat. In fact, it is fundamentally more difficult to make predictions for fuel mixtures with just a few components, as they can exhibit strong sensitivity toward fuel composition variations. To amplify the above point, we compare the distributions of laminar flame speed S_u° computed for 5- and 14-component random fuel mixtures in air at 403 K and 1 atm for two equivalence ratios. As shown in Fig. 9, the 2σ value in S_u° computed for 5-component mixtures is ± 4–5 cm/s, whereas the 2σ value of 14-component fuel mixtures becomes essentially negligible (2σ ó = ± 1.7 cm/s for $\phi = 1$ and ± 2.6 cm/s for $\phi = 1.3$). Not surprisingly, the S_u° values measured for a typical jet fuel (Jet A, POSF10325) are fairly close to the respective Monte Carlo results, as shown in Fig. 9. The above analyses suggest that if one is to adopt the surrogate fuel approach, the best jet fuel surrogate mixture is probably a random sample of more than 13 hydrocarbon compounds, as any of such hydrocarbon mixture would exhibit combustion chemistry behaviors that closely mimic real, multi-component fuels. While the above observation probably applies also to gasoline and diesel fuels, the presence of olefins and oxygenates (e.g., ethanol) in these fuels would require future investigation in order to make a similar conclusion.

The fuel mixtures sampled above probably exhibit compositional variations larger than those of real liquid fuels. For example, the sampling does not consider the more limited variations in the H/C ratio and lower heating value (LHV) that are a part of the real fuel specification. For this reason, our subsequent tests add some constraints to the sampling. These tests used H/C = 2.0 ± 0.1 and LHV = 43.9 ± 0.3 MJ/kg, both of which are close to the respective values of jet fuels. Figure 10 shows the distributions of key intermediates from the pyrolysis of 16-component fuel-mixtures at 1 atm pressure and 1300 K initial temperature. The 12 pyrolysis products, arranged in a decreasing mean concentration, are all that we need to consider as they account for almost the entire de-

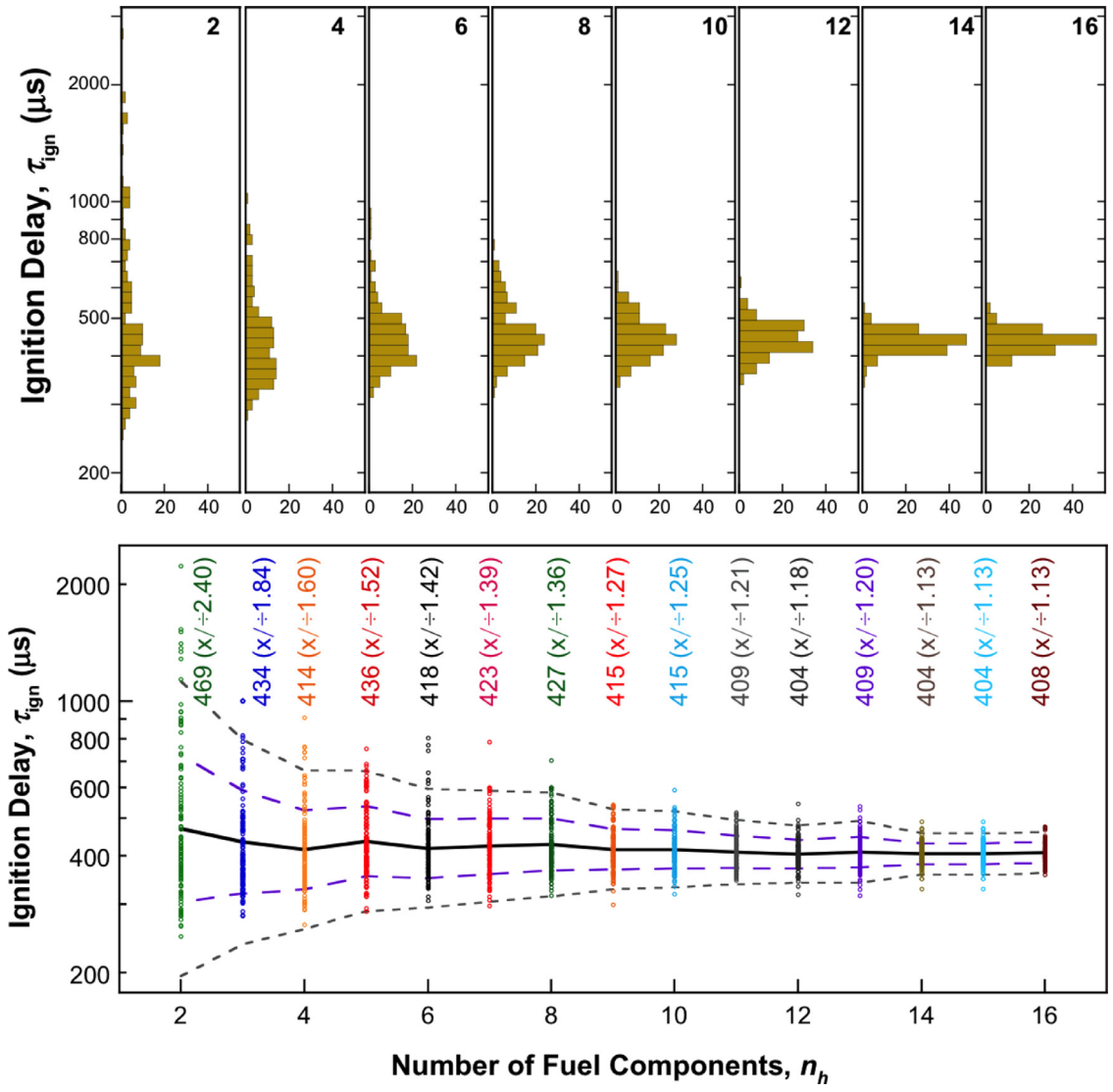

Fig. 8. Histogram of (top panel) and actual calculated (lower panel) ignition delay time (τ_{ign}) of 6% (wt) of n_h-component fuel mixtures randomly sampled from Table 1 in air at an initial temperature of 1300 K and 1 atm pressure under the isochoric condition. The top panel shows results of even n_h (=2, 4, ...,16) values only. The values in the lower panels are the mean and two-standard deviation factor. For the $n_h = 16$ case, the variation in the ignition delay is purely due to concentration variations of the 16 hydrocarbon components.

composed fuel mass. Among them, propyne/allene, acetylene, and 1,3-butadiene are minor products and in any case, are produced from C_3H_6, C_2H_4 and 1-C_4H_8, respectively. Hence, there are nine species in all to consider: C_2H_4, H_2, C_3H_6, *i*-C_4H_8, CH_4, C_2H_6, 1-C_4H_8, C_7H_8 and C_6H_6. Ethane (C_2H_6) is produced from the recombination of the CH_3 radicals, and as such it is accounted for through the foundational fuel chemistry model. Furthermore, Fig. 10 shows that the concentrations of a majority of species are quite narrowly distributed. The narrow distributions are of course the leading cause for the invariance observed for the ignition delay time and flame speed, because the oxidation of these pyrolysis products and the resulting radical growth and heat release are ultimately responsible for the various combustion responses.

The small sensitivity of the pyrolysis product distributions to the fuel composition is strongly supported by experiments. Figure 11 shows the average product yields at around 20 ms of reaction time of the three jet fuels in Fig. 1 undergoing pyrolysis at 1140 K and 1 atm in a flow reactor. The key species are always the same and the number of these species is small. Since the flow reactor experiments used vitiated air, there is an appreciable amount of water in the background gas. The presence of water impacts the fuel decomposition rate and methane production due to the reactions $H + H_2O = OH + H_2$ and $CH_3 + H_2 = CH_4 + H$, but it does not affect the distribution of other products or the number of such products at the reaction time shown in Fig. 11. It is important to note that the flow reactor experiments identified C_4H_8 to be mostly 1-C_4H_8, yet the Monte Carlo results show the yield of *i*-C_4H_8 to be twice that of 1-C_4H_8. Since *i*-C_4H_8 is only produced from the highly branched iso-paraffins (neohexane and 2,2,4-trimethylpentane), the smaller *i*-C_4H_8 production suggests that highly branched *iso*-paraffins are not abundant in the Jet A studied—an issue that will be explored in a separate study.

6. The HyChem approach

The approach builds on the observations and rules discussed above. It combines an experimentally constrained, “one-species” fuel pyrolysis model with a detailed foundational fuel chemistry model for the oxidation of the pyrolysis fragments. The USC Mech II [51] is comprised of 111 species and 784 reaction and is used here for this purpose. Detailed application of the approach to several jet fuels will be discussed in a companion paper [19]. Here we

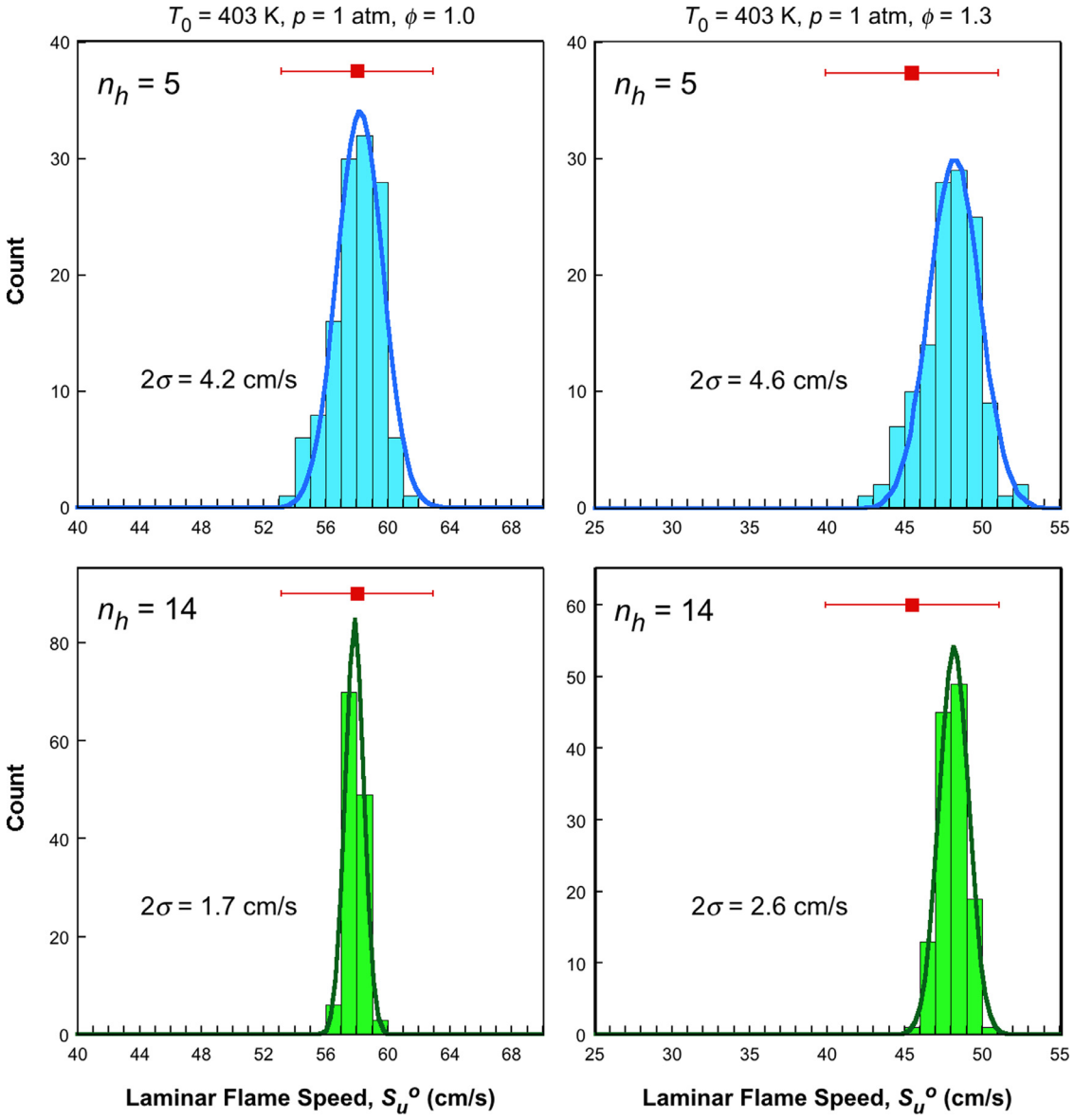

Fig. 9. Histograms and distributions of laminar flame speed computed for randomly sampled 5- and 14-component fuel–air mixtures at 1 atm and the equivalence ratios of 1.0 (left panel) and 1.3 (right panel). The unburned gas temperature is 403 K. The square symbols and their associated error bars are the flame speed values measured in the present work for a typical Jet A and their 2-standard deviations.

Table 2
Key properties of the Jet A fuel (A2) studied [4].

Fuel	Average formula	H/C ratio	MW (g/mol)	LHV (MJ/kg)	H_v (MJ/kg)	Constituent HC classes and composition (mass%)			
						n-paraffin	*iso*-paraffin	cycloparaffin	aromatics
A2	$C_{11.4}H_{21.7}$	1.90	158.6	43.1	0.36	20.0	29.4	31.9	18.7

discuss the underlying assumptions and illustrate the applicability of the method for one conventional kerosene, a Jet A fuel designated here as the A2 jet fuel (designated by the National Jet Fuels Combustion Program). Its hydrocarbon-class composition is shown in Fig. 1 and key properties are presented in Table 2.

Key assumptions are:

(1) For high-temperature combustion of single-component or multi-component fuels comprised of sufficiently large hydrocarbons, the thermal decomposition of the fuel molecules proceeds before the oxidation of the decomposition products even with oxygen presence; as such the two processes may be treated in a decoupled manner.
(2) The thermal decomposition of the fuel is not rate limiting and can be treated without needing to know the details at the level of elementary reactions; and the relevant reactions may be treated in a manner similar to the *n*-hexane example discussed in Section 4.2.
(3) The number of decomposition products needed to describe subsequent combustion behavior is substantially smaller than that in the original multi-component fuel. From earlier discussion, these are: C_2H_4, C_3H_6, C_4H_8 (1-butene and *iso*-

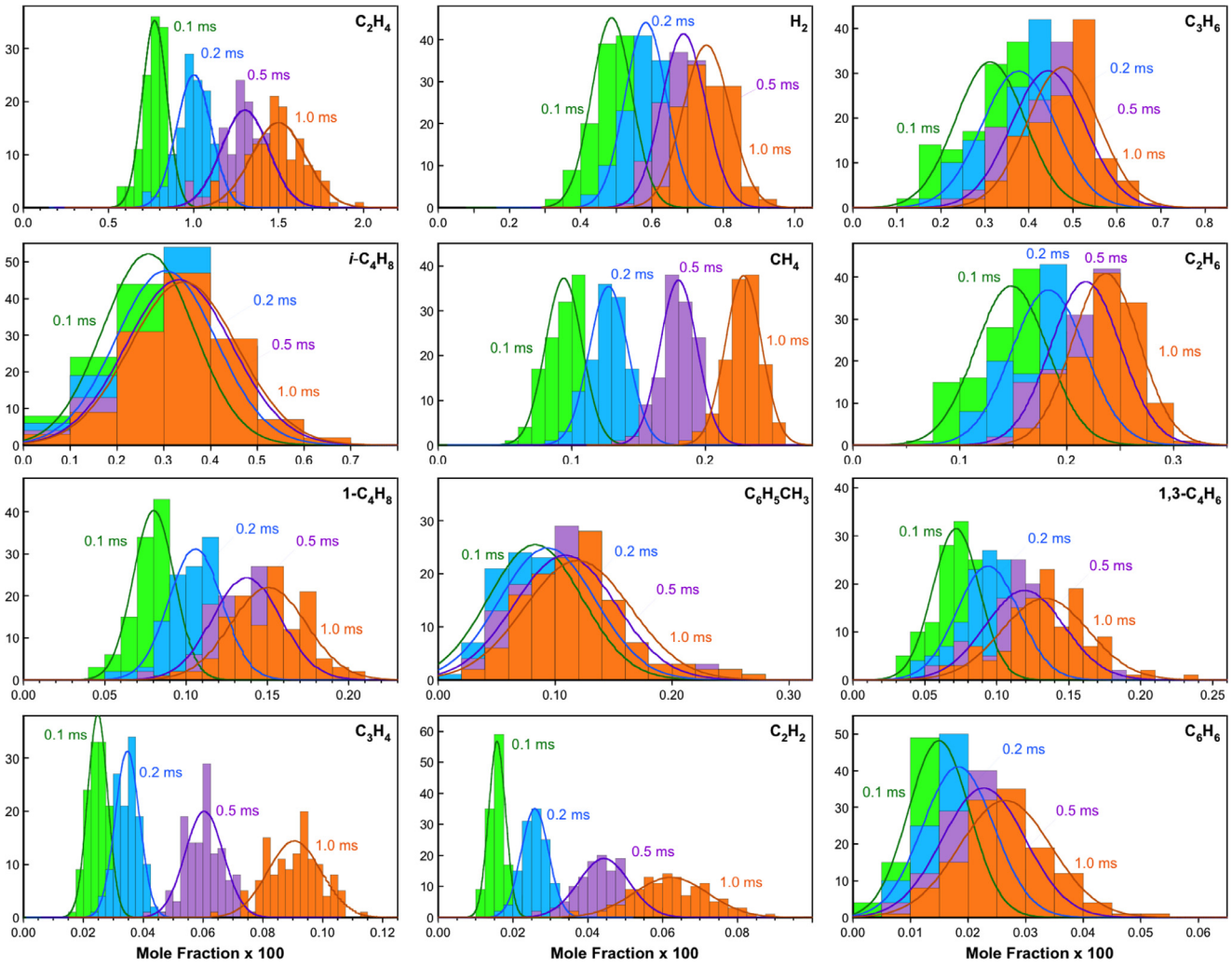

Fig. 10. Product distributions computed for the pyrolysis of 128 samples of 16-compoennt fuel–N_2 mixtures (MW = 113 ± 7 g/mol, H/C = 2.0 ± 0.1 and LHV = 43.9 ± 0.3 MJ/kg) under adiabatic and isobaric conditions. The pressure is 1 atm and initial temperature is 1300 K. The fuel mass loading is 6%.

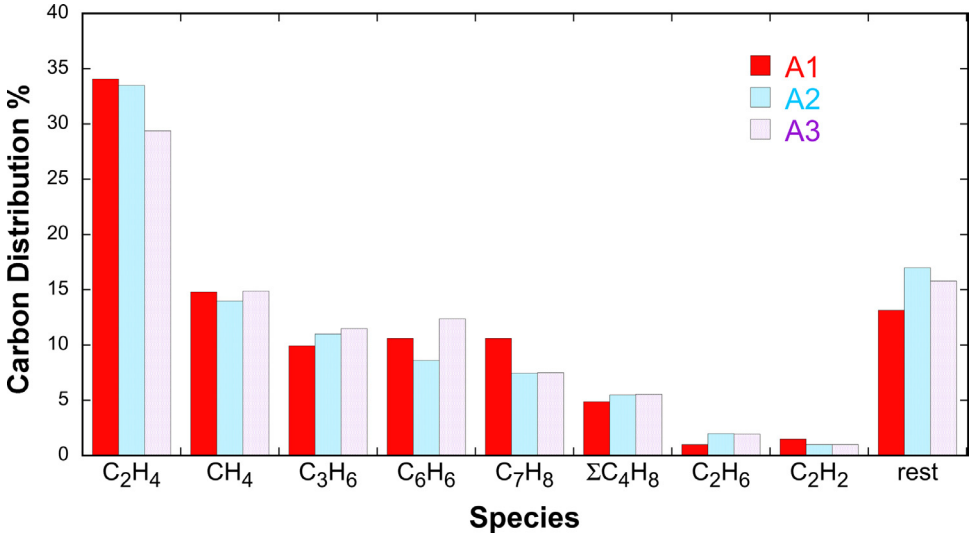

Fig. 11. Carbon distributions measured in a flow reactor for the pyrolysis products of the three jet fuels shown in Fig. 1 (t = ~20 ms, p = 1 atm, T = 1140 K and 300 ppm fuel). C_4H_8 represents a mixture of 1-C_4H_8 and i-C_4H_8 with the 1-C_4H_8-to-i-C_4H_8 ratio around 2-to-1. The "rest" is primarily unreacted fuel.

butene), CH_3, CH_4, H, H_2, C_6H_6, and C_7H_8. It is further assumed that acetylene, propyne/allene and 1,3-butadiene are produced primarily from the further reaction of C_2H_4, C_3H_6, and the C_4H_8 isomers.

(4) The pyrolysis and oxidation of decomposed products is rate limiting; for this reason, it must be treated by a detailed reaction model.

(5) The combined reaction model is comprised of a lumped model for fuel pyrolysis and a foundational, detailed fuel chemistry model for the pyrolysis and oxidation of H_2, CO, C_{1-4} hydrocarbons, benzene and toluene.

6.1. Lumped fuel pyrolysis model

Any hydrocarbon may be represented by the chemical formula C_mH_n. The fuel can be multi-component, in which case the formula represents some average composition of the fuel. The HyChem model expresses the thermal or oxidative thermal decomposition of the fuel in two separate reaction steps:

$$C_mH_n \rightarrow e_d(C_2H_4 + \lambda_3 C_3H_6 + \lambda_4 C_4H_8) + b_d[\chi C_6H_6 + (1-\chi)C_7H_8] + \alpha H + (2-\alpha)CH_3 \quad \text{(R1)}$$

$$C_mH_n + R \rightarrow RH + \gamma CH_4 + e_a(C_2H_4 + \lambda_3 C_3H_6 + \lambda_4 C_4H_8) + b_a[\chi C_6H_6 + (1-\chi)C_7H_8] + \beta H + (1-\beta)CH_3 \quad \text{(R2)}$$

where $R = H$, CH_3, O, OH, O_2 and HO_2. Reaction (R1) represents the C–C fission in the fuel "molecule," with the resulting products similarly specified as those of the H-abstraction reaction (R2) followed by ®-scission. Reaction (R2) is written in a similar fashion as that in the case study of *n*-hexane (Section 4.2). Hence, we have one thermal decomposition reaction and six H-abstraction reactions written in the lumped form.

6.2. Elemental conservation

Parameters α and β represent the number of H atoms produced per C_mH_n consumed in reactions (R1) and (R2), respectively. They are bound by $\alpha \in [0, 2]$ and $\beta \in [0, 1]$, and as such reaction (R1) produces net two free radicals, and reaction (R2) produces no net free radicals. Additionally, the reactions were purposefully cast in the form that some of the stoichiometric parameters can be determined directly from suitable experiments.

Here, parameters α, β, χ, λ_i and γ are treated as independent variables, whereas e_d, e_a, b_d and b_a are dependent variables from elemental conservation:

$$e_d = \frac{\left[-(4-\chi)m + \frac{(7-\chi)}{2}n + 3\alpha + \chi - 13\right]}{3(2+3\lambda_3+4\lambda_4)},$$

$$e_a = \frac{\left[-(4-\chi)m + \frac{(7-\chi)}{2}n + 3\beta - (10-\chi)\gamma - (10-\chi)\right]}{3(2+3\lambda_3+4\lambda_4)},$$

$$b_d = \frac{1}{3}\left(m - \frac{n}{2} + 1\right)$$

$$b_a = \frac{1}{3}\left(m - \frac{n}{2} + \gamma + 1\right).$$

The physical significances of the independent stoichiometric parameters and their bounds are explained in Table 1 of the companion paper [19]. Briefly, λ_3 is the C_3H_6-to-C_2H_4 ratio; λ_4 is the C_4H_8-to-C_2H_4 ratio, and χ is the ratio of C_6H_6 to the sum of C_6H_6 and $C_6H_5CH_3$. In some cases, isomers of C_4H_8 must be considered: 1-C_4H_8 and *i*-C_4H_8, in which case, $\lambda_4 = \lambda_{4,1} + \lambda_{4,i}$, corresponding to the coefficients for 1-C_4H_8 and *i*-C_4H_8, respectively. γ is zero in principle as it measures the yield of CH_4 beyond what is produced from H-abstraction by CH_3 in reaction R2. Here, we retain the γ parameter for generality, but its value is always close to zero, as expected.

The elemental balances set bounds to the variation of the stoichiometric coefficients and thus the product distribution. In general, real fuels have H/C ratios ~ 2. Since all alkenes produced have H/C ratio of 2, the yield of CH_4 must be correlated with C_6H_6 and C_7H_8 yields. A larger CH_4 yield must always be associated with larger C_6H_6 and/or C_7H_8 yields. As will be shown, below 1400 K, the yields of the pyrolysis products always reach respective plateau values regardless whether or not oxygen is present. Consequently, the plateau values may be used as the initial estimates for λ_3, λ_4, and χ. Determining the values of α, β, and γ is somewhat more involved, as these parameters are coupled with the rate coefficients k_1 and $k_{2,i}$ ($i = 1, 6$). With carefully designed experiments over a suitable range of conditions, it is possible to make reasonably good estimates for these parameters in an inverse problem. All of the rate coefficients are temperature dependent. Hence, the actual number of parameters to be determined is larger than nine. Yet recognizing that the fuel molecules usually decompose fast and the rate is not critical to subsequent radical buildup and heat release, the difficulty in choosing and fitting the rate coefficients should not be critical to obtaining a predictive model. Rather, an accurate determination of the stoichiometric parameters is more critical to the predictive accuracy of the model.

6.3. Experiments

Three different types of the experiment were used to estimate the stoichiometric parameters and rate coefficients and test the model. Shock tube studies yield two types of data: i) C_2H_4, CH_4 and in some cases, C_3H_6 time histories in pyrolysis and oxidative pyrolysis around 12 bar, ii) ignition delay from 1 to 15 bar at around unity equivalence ratio. These experiments were carried out over a range of temperatures relevant to the high-temperature chemistry. A broader range of equivalence ratio has been tested for the ignition delay as discussed in ref. [19]. The flow reactor generates oxidative pyrolysis time history data for a more complete set of species to ensure carbon balance, although the operable temperature range of the flow reactor is narrower than that of the shock tube and the experiment is limited to atmospheric pressure for the current study. The counterflow flame configuration generates S_u° at ambient pressure. K_{ext}'s of non-premixed flames were also considered. The experimental data are used for two separate purposes. Speciation data are used for obtaining the model parameters; and global combustion properties (τ_{ign}, S_u° and K_{ext}) are employed for testing the model. Additional literature data are available for Jet A and other types of kerosene, including shock tube ignition delay [52–56], laminar flame speed [57–60], counterflow laminar flame extinction and/or ignition [59,61–65]. Attempts have been made to test the HyChem models against some of these data, as will be discussed in the companion paper [19].

6.4. Model development

6.4.1. Thermochemical and transport data

The A2 fuel has an average molecular formula of $C_{11.4}H_{21.7}$. Since combustion codes can usually deal with integer molecular formula only, we approximate it as $C_{11}H_{22}$. Because of this simplification, experiment-model comparisons must be made on the basis of equal fuel mass fraction, rather than mole fraction. The standard-state enthalpy of formation was calculated from the LHV value listed in Table 2; and the enthalpy of vaporization was estimated ($H_v = 0.36$ MJ/kg. see, the companion paper [19] for details). The specific heat and entropy were estimated from a surrogate mixture containing 23.42% (mol) 1,2,4-trimethylbenzene, 26.09% *iso*-dodecane, 19.33% *n*-undecane and 31.16% *n*-pentyl-cyclohexane.

Table 3
Thermochemical property values of the A2 fuel.

$\Delta_f h^\circ_{298}$ (kcal/mol)	s°_{298} (cal/mol-K)	$c_p(T)$ (cal/mol-K)				
		300 K	500 K	1000 K	1500 K	2000 K
−66.9	121.1	54.5	84.7	131.6	152.5	164.4

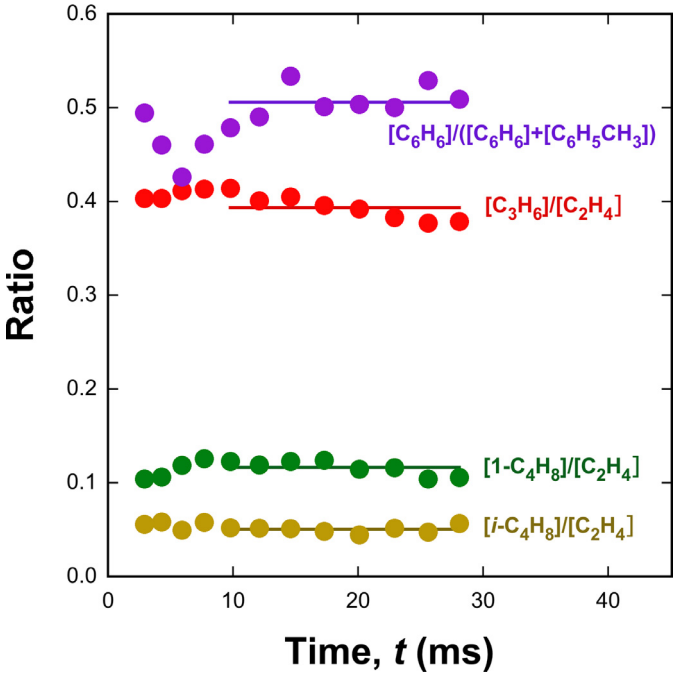

Fig. 12. Measured ratios of key species concentrations during A2 oxidation (314 ppm A2 in a vitiated oxygen–nitrogen mixture at the unity equivalence ratio) in a flow reactor at 1030 K temperature and 1 atm pressure. Symbols are experimental data; lines are drawn to guide the eye.

The composition matches the mean molecular weight, H/C ratio, and compound classes of the A2 fuel. Table 3 lists the thermochemical property values adopted for the A2 fuel.

The diffusion coefficients of the fuel are based on a series of recent studies in which we studied the effect of non-elastic, non-spherical potential of long-chain molecules and dependence of the counter-flow flame extinction on the molecular diffusivity [66–68]. Although a more fundamental study is needed, we assume that for the purpose of calculating the transport properties, the effective intermolecular potential parameters of the fuel are represented by that of *n*-undecane (*n*-$C_{11}H_{24}$) for the A2 fuel. When a range of jet fuels were examined (to be discussed in the companion paper [19]), it was found that a suitable approach is to describe the potential parameters of a real, C_mH_n fuel by those of a C_mH_{2m+2} *n*-alkane. The HyChem model of A2 fuel, including the thermochemical and transport data are provided by a webpage link in the Supplementary Materials.

6.4.2. Stoichiometric and rate parameters

The flow reactor experiment was carried out at 314 ppm A2 diluted in a vitiated oxygen-nitrogen mixture at unity equivalence ratio, 1030 K temperature and 1 atm pressure. Figure 12 shows that the various ratios related to parameters λ_3, $\lambda_{4,1}$, $\lambda_{4,i}$ and χ are indeed constant after the initial few milliseconds. The average values for $[C_3H_6]/[C_2H_4]$, $[1\text{-}C_4H_8]/[C_2H_4]$, $[i\text{-}C_4H_8]/[C_2H_4]$ and $[C_6H_6]/([C_6H_6]+[C_6H_5CH_3])$ measured after 10 ms to the end of the reactor (29 ms) are around 0.4, 0.12, 0.05 and 0.51, respectively. Table 4 lists the actual stoichiometric coefficients. Because of the short time scales of conversion relative to the long residence time in the flow reactor, C_3H_6 and $1\text{-}C_4H_8$ continue to be converted to C_2H_4 as they form. Consequently, the actual values for λ_3 and $\lambda_{4,1}$ are larger than the measured product ratios and equal to 0.47 and 0.15 respectively. Interestingly, these values are not very different from those of *n*-hexane: 0.38 and 0.25, i.e., Eq. (2) using $a = 0.44$. The larger λ_3 value is consistent with our expectation, as the *iso*-alkane and cycloparaffin compounds in the A2 fuel would produce more C_3H_6 than any *n*-alkane compounds. The $\lambda_{4,i}$ and χ values are identical to the measured $[i\text{-}C_4H_8]/[C_2H_4]$ and $[C_6H_6]/([C_6H_6]+[C_6H_5CH_3])$ values owing to the stability of $i\text{-}C_4H_8$ and the negligible rate of the mutual conversion between benzene and toluene.

Table 4
Fuel pyrolysis model parameters of A2 ($C_{11}H_{22}$)[a].

Stoichiometric parameter	Value		
a	0.5		
β	0.3		
γ	0.45		
λ_3	0.47		
$\lambda_{4,1}$	0.15		
$\lambda_{4,i}$	0.05		
χ	0.51		
Rate parameters[b] ($k = A\,T^n\,e^{-B/RT}$)			
reaction	A	n	B
k_1	1.5×10^{27}	−2.58	87,700
$k_{2,H}$	7.7×10^{-2}	4.76	1295
k_{2,CH_3}	3.2×10^{-7}	5.95	5750
$k_{2,O}$	8.9×10^{1}	3.86	765
$k_{2,OH}$	3.0×10^{9}	1.02	213
k_{2,O_2}	1.8×10^{15}	0.06	44,500
k_{2,HO_2}	7.0×10^{4}	2.94	12,810

[a] USC Mech II is used as the foundational fuel chemistry model. [b]Units are mol, cm, s, and cal/mol.

The rate coefficients were estimated initially from the analogous reactions from JetSurF 2.0, and then along with the stoichiometric parameters, were fitted to the shock tube and flow reactor species data. The final reaction model is provided in the Supplementary Materials as a webpage link. The flow rector data shown in Fig. 12 are the most useful for estimating the stoichiometric coefficients γ, λ's, and χ. The C_2H_4 and CH_4 CH_4 time-history measurements acquired in the shock tube (Figs. 13 and 14) are the most relevant to the rate parameters and the α and β values. Figure 13 shows an example of the model fits and experimental data for the time histories of C_2H_4 and CH_4. Summary comparisons are presented in Fig. 14 at two representative reaction times over the range of T_5 value tested, all at 12.4 atm nominal pressure. Both figures show the impact of temperature uncertainty of 15 K (~1%) on the C_2H_4 and CH_4 yields. The measurement uncertainties for the C_2H_4 and CH_4 yields acquired at high pressures and based on the 2-wavelength analysis assumptions are typically ± 20%. Additional details can be found in [19]. Figure 15 shows the comparison of the experimental and modeled C_2H_4 yields at 0.5 ms reaction time of A2 oxidative pyrolysis at unity equivalence ratio and pyrolysis over a range of temperature and 1.6 atm nominal pressure. The results show that in oxidative pyrolysis the C_2H_4 yield at 0.5 ms is slightly higher than that from pyrolysis, because of faster radical pool growth in oxidation than in pyrolysis. The absolute deviations between the experiment and model probably reflect the experimental accuracy as these are rather difficult measurements.

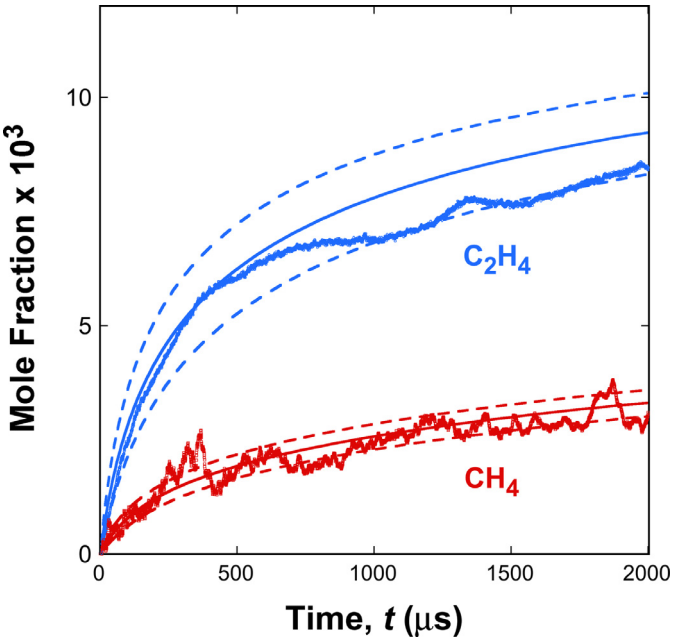

Fig. 13. Typical time histories of C_2H_4 and CH_4 measured and simulated from thermal decomposition of 0.73 % (mol) A2 fuel in argon in shock tube at $T_5 = 1196$ K and $p_5 = 12.5$ atm. The dashed lines are simulations bracketing the ± 15 K temperature uncertainty. Additional details of the experimental data can be found in ref [19].

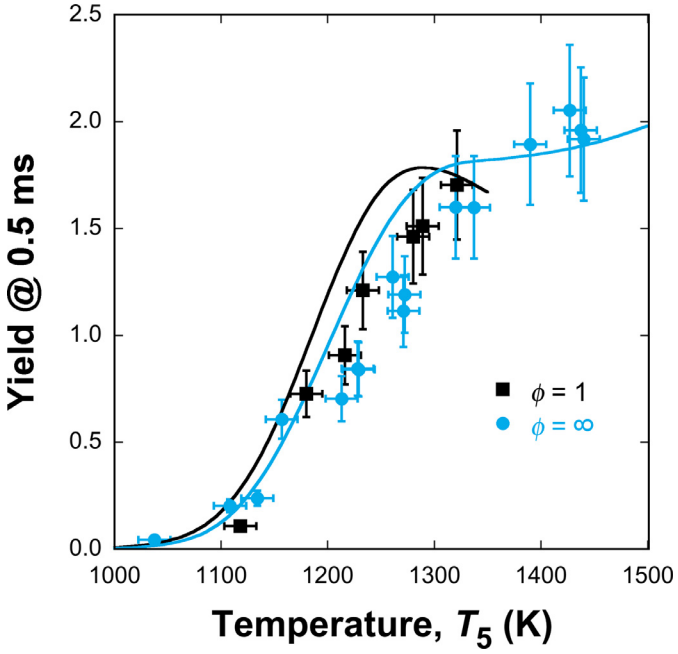

Fig. 15. Yields of C_2H_4 measured (symbols) and simulated (lines) at 0.5 ms reaction time from shock tube oxidation ($\phi = 1$) and pyrolysis of 0.4 % (mol) A2 with argon as the balance gas at $p_5 = 1.6$ atm. Error bars represent ± 15 K in temperature uncertainty and experimental uncertainties of C_2H_4 concentrations. Additional details of the experimental data can be found in ref [19].

6.5. Test against global combustion data

The HyChem model thus derived is available in the Supplementary Materials along with thermochemical and transport databases. Here, we show the model test results against global combustion properties. Figure 16 shows comparisons of the experimental and simulated ignition delays of five mixtures over a range of pressure, concentration, type of diluent (Ar vs. N_2) and to an extent, the equivalence ratio. Clearly, the model is capable of capturing the experimental τ_{ign} rather well. The largest discrepancy is for the A2-21%O_2–Ar mixture at high pressures and lower temperatures, and the discrepancy is likely the result of the Negative-Temperature Coefficient (NTC) chemistry not yet considered in the HyChem model. An NTC-enabled HyChem model for the same fuel will be presented in [19]. Figure 17 shows the comparisons of S_u° and K_{ext}. Again, the HyChem model reproduces the data closely.

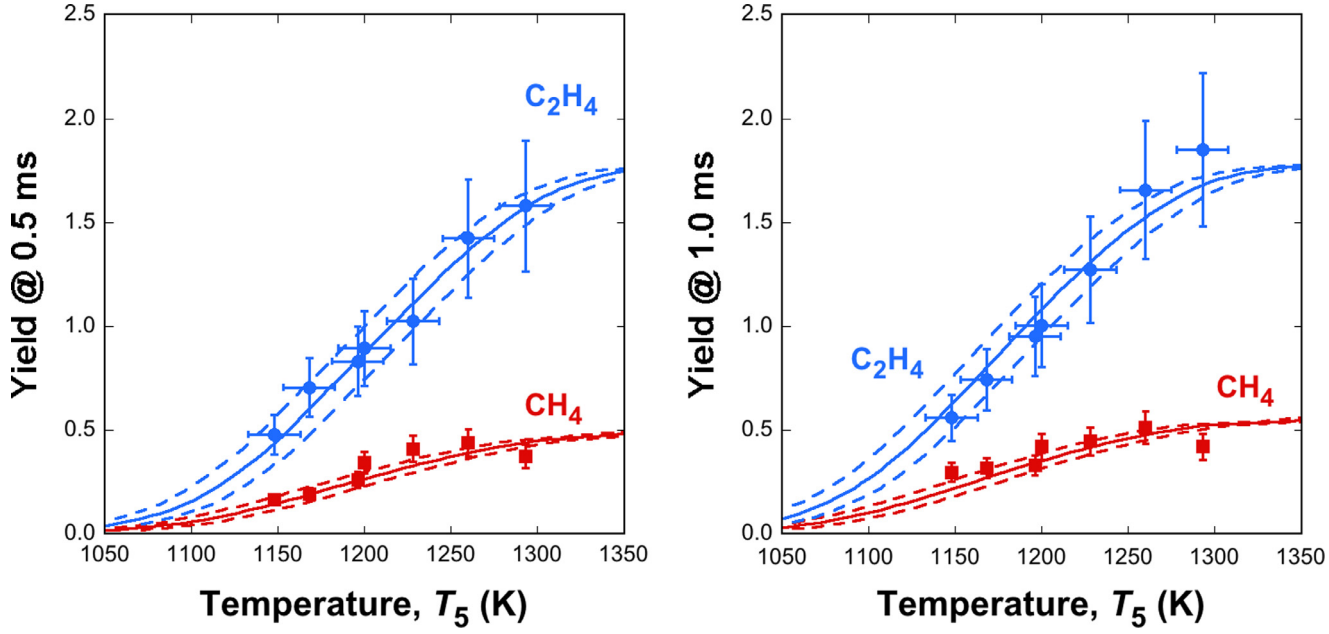

Fig. 14. Yields of C_2H_4 and CH_4 measured (symbols) and simulated (lines) from thermal decomposition of 0.73% (mol) A2 fuel in argon in shock tube at $p_5 = 12.4$ atm. The dashed lines are simulations bracketing the ± 15 K temperature uncertainty. Error bars on the data represent ± 15 K in temperature uncertainty and experimental uncertainties of C_2H_4 and CH_4 concentrations. Additional details of the experimental data can be found in ref [19].

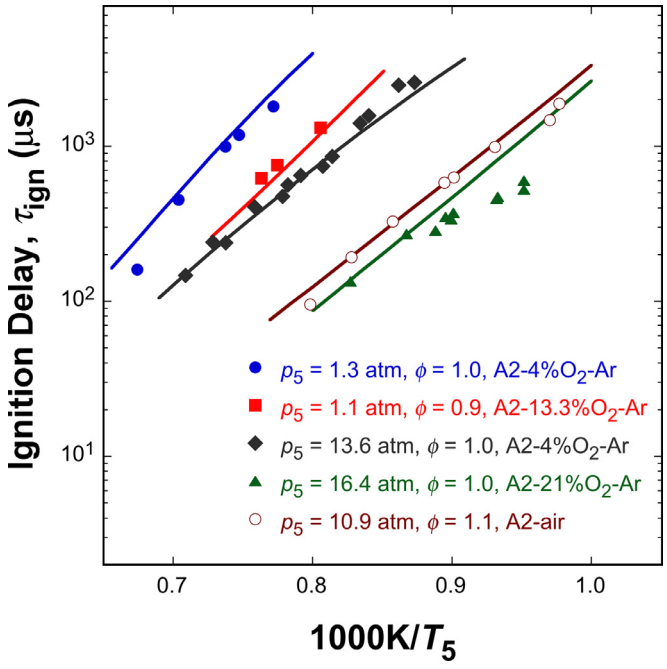

Fig. 16. Measured (symbols) and simulated (lines) ignition delay times of the A2 fuel under various mixture conditions. Additional details of the experimental data can be found in ref [19].

6.6. Is HyChem the traditional lumping approach?

Chemical lumping is a simplification method of detailed kinetic modeling that has been championed and applied extensively to chemical engineering research and combustion chemistry modeling by Ranzi and others for many years (see, e.g., [16,69,70]). The HyChem approach is similar to chemical lumping in some way, but the two approaches differ in the following aspects:

(1) The HyChem approach does not require the availability of a detailed reaction mechanism and model to derive a predictive reaction model of a reduced order. Rather, it relies on a physical, cause-and-effect understanding and as importantly, advanced diagnostics to reliably achieve model predictability.

(2) The HyChem approach bypasses the need to use surrogate mixtures and detailed reaction models. It probes real-fuel combustion process and properties and advances the modeling capability from these properties directly.

7. Conclusions

The following conclusions can be made from the experiments and analyses presented herein:

1. For combustion processes occurring above the temperature where the NTC chemistry is relevant, large hydrocarbon fuels undergo pyrolysis first, followed by the oxidation of pyrolysis products. The decoupled description is applicable to phenomena governed by radical pool buildup and in flames.
2. The second step, i.e., the oxidation of pyrolysis products, is rate limiting. Hence, the composition of the decomposed products determines the overall oxidation rate and consequently, many of the global combustion properties, from ignition delay to flame propagation and extinction.
3. The number of thermal decomposition products is small, especially compared to the number of components in distillate fuels. Key species are C_2H_4, CH_4, C_3H_6, 1-C_4H_8, i-C_4H_8, H_2, benzene and toluene, where CH_4 and H_2 derive from the H-abstraction by the CH_3 radical and H atom, respectively.
4. The combustion chemistry of real, multi-component fuels is not more complex than a single-component fuel. In fact, with the exception of the sooting propensity, the multi-component nature of the fuel largely removes the composition dependency of the combustion properties due to the underlying statistical factor, in such a way that real engines can tolerate pump-to-pump, region-to-region, or distiller-to-distiller fuel composition variations.
5. Following the physical understanding outlined above, a Hybrid Chemistry (HyChem) approach was formulated. It combines experimentally constrained, lumped reaction steps for fuel thermal decomposition and oxidative pyrolysis with detailed reaction chemistry for the pyrolysis and oxidation of the fuel decomposition products. A HyChem model, formu-

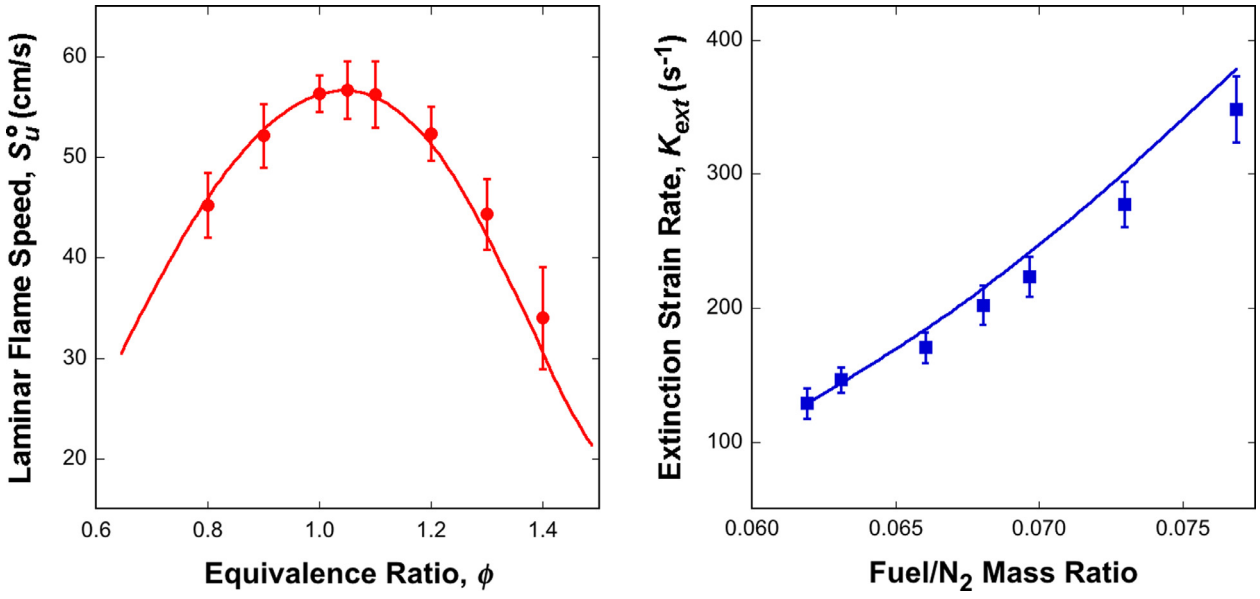

Fig. 17. Experimental (symbols) and simulated (lines) laminar flame speed of A2 in air (403 K unburned gas temperature) and extinction strain rate of non-premixed A2/N_2 against O_2 (the A2/N_2 jet temperature is 473 K, and O_2 temperature is 300 K), all at 1 atm pressure. Additional details of the experimental data can be found in ref [19].

lated and developed here for a typical Jet A fuel, is shown to reproduce its global combustion properties very well, including ignition delay time, laminar flame speed and non-premixed flame extinction.

Overall, the effort outlined herein illustrates the importance of physical understanding in removing many of the difficulties in modeling real fuel combustion chemistry. Many of the complexities associated with real, multi-component fuels were only perceived, but never directly tested or proved. Lastly, in subsequent studies, we will show that the HyChem model can be reduced to around a total of ~30 species to describe the entire high-temperature combustion chemistry of many real distillate jet fuels, thus enabling turbulent combustion modeling of real fuel, real combustor processes. Fuel distillate-fraction dependent reaction models, if necessary, can be easily developed by directly experimenting on a particular fraction. Thus, the HyChem approach offers the possibility of a unified approach to spray evaporation and reaction kinetics, thus removing one of the critical fundamental difficulties associated with the surrogate fuel approach. Even without treating the distillate-fraction dependent reaction kinetics, HyChem models have been shown to advance our capability in predicting real-fuel combustion behaviors in turbulent combustors (see, e.g., [71,72]).

Acknowledgment

The authors acknowledge Dr. Sayak Banerjee for obtaining some of the flow reactor data. The significant technical involvement by the AFOSR program manager, Dr. Chiping Li, is acknowledged. This research was funded by the Air Force Office of Scientific Research under grant numbers FA9550-14-1-0235 (CTB, RKH and HW), FA9550-16-1-0195 (CTB, RKH and HW), FA9550-12-1-0472 (HW), FA9550-15-1-0409 (FNE), and FA9550-16-1-0079 (KB). The work was also supported by the National Aeronautics and Space Administration (NASA) under agreement numbers NNX15AV05A (HW) and NNX15AU96A (TL) and by the Federal Aviation Administration Office of Environment and Energy as a part of ASCENT Projects 26 and 35 under FAA Award Numbers 13-CAJFE-SU-006 (HW) and 13-C-AJFE-SU-016 (RKH). Any opinions, findings, and conclusions or recommendations expressed in this material are those of the authors and do not necessarily reflect the views of the FAA or other ASCENT sponsors.

Supplementary materials

Supplementary material associated with this article can be found, in the online version, at doi:10.1016/j.combustflame.2018.03.019.

References

[1] W. Dabelstein, A. Reglitzky, A. Schütze, l. Reders, Automotive fuels, Ullmann's encyclopedia of industrial chemistry, Wiley-VCH, Weinheim, 2007.
[2] Aviation Fuels–Technical Review, Chevron Products Company, San Ramon, CA 2007.
[3] World Jet Fuel Specifications, ExxonMobile Aviation, Surrey 2005.
[4] T. Edwards, Personal Communication, 2015.
[5] A. Violi, S. Yan, E. Eddings, A. Sarofim, S. Granata, T. Faravelli, E. Ranzi, Experimental formulation and kinetic model for JP-8 surrogate mixtures, Combust. Sci. Technol 174 (2002) 399–417.
[6] T. Edwards, M. Colket, N.P. Cernansky, F.L. Dryer, F.N. Egolfopoulos, D. Friend, C.K. Law, D. Lenhert, P. Lindstedt, H. Pitsch, A. Sarofim, K. Seshadri, M. Smooke, W. Tsang, S. Williams, Development of an experimental database and kinetic models for surrogate jet fuels, 45th AIAA Aerospace Sciences Meeting and Exhibit, Reno, NV, 2007 AIAA Paper No. 2007-770.
[7] E.G. Eddings, S. Yan, W. Ciro, A.F. Sarofim, Formulation of a surrogate for the simulation of jet fuel pool fires, Combust. Sci. Technol 177 (2005) 715–739.
[8] H.R. Zhang, E.G. Eddings, A.F. Sarofim, Criteria for selection of components for surrogates of natural gas and transportation fuels, Proc. Combust. Inst 31 (2007) 401–409.
[9] M. Colket, T. Edwards, S. Williams, N.P. Cernansky, D.L. Miller, F.N. Egolfopoulos, F.L. Dryer, J. Bellan, P. Lindstedt, K. Seshadri, Identification of target validation data for development of surrogate jet fuels, 46th AIAA Aerospace Sciences Meeting and Exhibit, Reno, NV, 2008 AIAA Paper No. 2008-972.
[10] S. Dooley, S.H. Won, M. Chaos, J. Heyne, Y. Ju, F.L. Dryer, K. Kumar, C.-J. Sung, H. Wang, M.A. Oehlschlaeger, A jet fuel surrogate formulated by real fuel properties, Combust. Flame 157 (2010) 2333–2339.
[11] J. Farrell, N.P. Cernansky, F.L. Dryer, C.K. Law, D. Friend, C. Hergart, R. McDavid, A. Patel, C.J. Mueller, H. Pitsch, Development of an experimental database and kinetic models for surrogate diesel fuels, SAE Technical Paper, (2007) paper No. 2007-01-0201.
[12] S. Dooley, S.H. Won, J. Heyne, T.I. Farouk, Y. Ju, F.L. Dryer, K. Kumar, X. Hui, C.-J. Sung, H. Wang, The experimental evaluation of a methodology for surrogate fuel formulation to emulate gas phase combustion kinetic phenomena, Combust. Flame 159 (2012) 1444–1466.
[13] S. Dooley, S.H. Won, S. Jahangirian, Y. Ju, F.L. Dryer, H. Wang, M.A. Oehlschlaeger, The combustion kinetics of a synthetic paraffinic jet aviation fuel and a fundamentally formulated, experimentally validated surrogate fuel, Combust. Flame 159 (2012) 3014–3020.
[14] F.L. Dryer, S. Jahangirian, S. Dooley, S.H. Won, J. Heyne, V.R. Iyer, T.A. Litzinger, R.J. Santoro, Emulating the combustion behavior of real jet aviation fuels by surrogate mixtures of hydrocarbon fluid blends: implications for science and engineering, Energy Fuel 28 (2014) 3474–3485.
[15] T.M. Lovestead, J.L. Burger, S. N., T.J. Bruno, Comprehensive assessment of composition and thermochemical variability by high resolution GC/QToF-MS and the advanced distillation-curve method as a basis of comparison for reference fuel development, Energy Fuel 30 (2016) 10029–10044.
[16] E. Ranzi, M. Dente, A. Goldaniga, G. Bozzano, T. Faravelli, Lumping procedures in detailed kinetic modeling of gasification, pyrolysis, partial oxidation and combustion of hydrocarbon mixtures, Prog. Energy Combust. Sci. 27 (2001) 99–139.
[17] S. Li, B. Varatharajan, F. Williams, Chemistry of JP-10 ignition, AIAA J. 39 (2001) 2351–2356.
[18] B. Varatharajan, M. Petrova, F. Williams, V. Tangirala, Two-step chemical-kinetic descriptions for hydrocarbon–oxygen-diluent ignition and detonation applications, Proc. Combust. Inst. 30 (2005) 1869–1877.
[19] R. Xu, K. Wang, S. Banerjee, J. Shao, T. Parise, Y. Zhu, S. Wang, A. Movaghar, D.J. Lee, R. Zhao, X. Han, Y. Gao, T. Lu, K. Brezinsky, F.N. Egolfopoulos, D.F. Davidson, R.K. Hanson, C.T. Bowman, H. Wang, A physics-based approach to modeling real-fuel combustion chemistry - II. Reaction kinetic models of jet and rocket fuels, Combust. Flame (2018) submitted for publication, doi:10.1016/j.combustflame.2018.03.021.
[20] B. Sirjean, E. Dames, D.A. Sheen, X.Q. You, C. Sung, A.T. Holley, F.N. Egolfopoulos, H. Wang, S.S. Vasu, D.F. Davidson, R.K. Hanson, H. Pitsch, C.T. Bowman, A. Kelley, C.K. Law, W. Tsang, N.P. Cernansky, D.L. Miller, A. Violi, R.P. Lindstedt, JetSurF I: a high-temperature chemical kinetic model of *n*-alkane oxidation, 2017. https://web.stanford.edu/group/haiwanglab/JetSurF/JetSurF1.0.
[21] H. Wang, E. Dames, B. Sirjean, D.A. Sheen, R. Tangko, A. Violi, J.Y.W. Lai, F.N. Egolfopoulos, D.F. Davidson, R.K. Hanson, C.T. Bowman, C.K. Law, W. Tsang, N.P. Cernansky, D.L. Miller, R.P. Lindstedt, JetSurF II: a high temperature chemical kinetic model of *n*-alkane (up to *n*-dodecane), cyclohexane, and methyl-, ethyl-, *n*-propyl and *n*-butyl-cyclohexane oxidation at high temperatures, 2017. http://web.stanford.edu/group/haiwanglab/JetSurF/JetSurF2.0/.
[22] D. Darcy, H. Nakamura, C. Tobin, M. Mehl, W. Metcalfe, W. Pitz, C. Westbrook, H. Curran, A high-pressure rapid compression machine study of *n*-propylbenzene ignition, Combust. Flame 161 (2014) 65–74.
[23] H. Nakamura, D. Darcy, M. Mehl, C.J. Tobin, W.K. Metcalfe, W.J. Pitz, C.K. Westbrook, H.J. Curran, An experimental and modeling study of shock tube and rapid compression machine ignition of *n*-butylbenzene/air mixtures, Combust. Flame 161 (2014) 49–64.
[24] M. Mehl, H.J. Curran, W.J. Pitz, C.K. Westbrook, Chemical kinetic modeling of component mixtures relevant to gasoline, European Combustion Meeting, 2009.
[25] H.J. Curran, P. Gaffuri, W. Pitz, C. Westbrook, A comprehensive modeling study of iso-octane oxidation, Combust. Flame 129 (2002) 253–280.
[26] R.J. Kee, F.M. Rupley, J.A. Miller, CHEMKIN: a general-purpose, problem-independent, transportable, FORTRAN chemical kinetics code package, Sandia Report SAND-89-8009, Sandia National Laboratories, Albuquerque, N.M., 1989.
[27] R.J. Kee, J.F. Grcar, M. Smooke, J. Miller, E. Meeks, PREMIX: a Fortran program for modeling steady laminar one-dimensional premixed flames, Sandia Report SAND85-8240, Sandia National Laboratories, Albuquerque, N.M., 1985.
[28] F. Egolfopoulos, Geometric and radiation effects on steady and unsteady strained laminar flames, Symp. (Int.) Combust. 25 (1994) 1375–1381.
[29] R.J. Kee, J.A. Miller, G.H. Evans, G. Dixon-Lewis, A computational model of the structure and extinction of strained, opposed flow, premixed methane–air flames, Symp. (Int.) Combust. 22 (1989) 1479–1494.
[30] M. Nishioka, C. Law, T. Takeno, A flame-controlling continuation method for generating S-curve responses with detailed chemistry, Combust. Flame 104 (1996) 328–342.
[31] S. Banerjee, R. Tangko, D.A. Sheen, H. Wang, C.T. Bowman, An experimental and kinetic modeling study of *n*-dodecane pyrolysis and oxidation, Combust. Flame 163 (2016) 12–30.
[32] D. Davidson, Y. Zhu, J. Shao, R. Hanson, Ignition delay time correlations for distillate fuels, Fuel 187 (2017) 26–32.
[33] T. Parise, D. Davidson, R. Hanson, Shock tube/laser absorption measurements of the pyrolysis of a bimodal test fuel, Proc. Combust. Inst. 36 (2017) 281–288.

[34] Y. Wang, A. Holley, C. Ji, F. Egolfopoulos, T. Tsotsis, H. Curran, Propagation and extinction of premixed dimethyl-ether/air flames, Proc. Combust. Inst. 32 (2009) 1035–1042.
[35] N. Peters, Multiscale combustion and turbulence, Proc. Combust. Inst. 32 (2009) 1–25.
[36] G. Joulin, P. Clavin, Linear stability analysis of nonadiabatic flames: diffusional-thermal model, Combust. Flame 35 (1979) 139–153.
[37] C.K. Law, Combustion physics, Cambridge University Press, Cambridge, UK, 2006.
[38] D. Davidson, Z. Hong, G. Pilla, A. Farooq, R. Cook, R. Hanson, Multi-species time-history measurements during *n*-heptane oxidation behind reflected shock waves, Combust. Flame 157 (2010) 1899–1905.
[39] D.A. Sheen, H. Wang, Combustion kinetic modeling using multispecies time histories in shock-tube oxidation of heptane, Combust. Flame 158 (2011) 645–656.
[40] T. Malewicki, K. Brezinsky, Experimental and modeling study on the pyrolysis and oxidation of *n*-decane and *n*-dodecane, Proc. Combust. Inst. 34 (2013) 361–368.
[41] D. Davidson, Z. Hong, G. Pilla, A. Farooq, R. Cook, R. Hanson, Multi-species time-history measurements during n-dodecane oxidation behind reflected shock waves, Proc. Combust. Inst. 33 (2011) 151–157.
[42] D. Haylett, D. Davidson, R. Cook, Z. Hong, W. Ren, S. Pyun, R. Hanson, Multi-species time-history measurements during *n*-hexadecane oxidation behind reflected shock waves, Proc. Combust. Inst. 34 (2013) 369–376.
[43] I. Glassman, Combustion, 3rd ed., Academic Press, San Diego, CA, 1996.
[44] H. Wang, M. Frenklach, A detailed kinetic modeling study of aromatics formation in laminar premixed acetylene and ethylene flames, Combust. Flame 110 (1997) 173–221.
[45] X. You, F.N. Egolfopoulos, H. Wang, Detailed and simplified kinetic models of *n*-dodecane oxidation: the role of fuel cracking in aliphatic hydrocarbon combustion, Proc. Combust. Inst. 32 (2009) 403–410.
[46] B. Sirjean, E. Dames, H. Wang, W. Tsang, Tunneling in hydrogen-transfer isomerization of *n*-alkyl radicals, J. Phys. Chem. A 116 (2011) 319–332.
[47] A. Ratkiewicz, T.N. Truong, Kinetics of the C–C bond beta scission reactions in alkyl radical reaction class, J. Phys. Chem. A 116 (2012) 6643–6654.
[48] K. Wang, C.T. Bowman, H. Wang, Kinetic analysis of distinct product generations in oxidative pyrolysis of four octane isomers, Proc. Combust. Inst. (2018) submitted for publication.
[49] M. Hazewinkel, Law of large numbers, Encyclopedia of mathematics, Springer, Netherlands, 2001.
[50] R. Xu, H. Wang, Principle of large component number in multicomponent fuel combustion – a Monte Carlo study, Proc. Combust. Inst. (2018) submitted for publication.
[51] H. Wang, X. You, A.V. Joshi, S.G. Davis, A. Laskin, F. Egolfopoulos, C.K. Law, USC Mech Version II: high-temperature combustion reaction model of $H_2/CO/C_1–C_4$ compounds. http://ignis.usc.edu/USC_Mech_II.htm, 2007.
[52] A.J. Dean, O.G. Penyazkov, K.L. Sevruk, B. Varatharajan, Ignition of aviation kerosene at high temperatures, 20th International Colloquium on Dynamics of Explosions and Reactive Systems, Montreal, Canada, 2005. Paper 87.
[53] M.S. Kahandawala, M.J. DeWitt, E. Corporan, S.S. Sidhu, Ignition and emission characteristics of surrogate and practical jet fuels, Energy Fuel 22 (2008) 3673–3679.
[54] S.S. Vasu, D.F. Davidson, R.K. Hanson, Jet fuel ignition delay times: shock tube experiments over wide conditions and surrogate model predictions, Combust. Flame 152 (2008) 125–143.
[55] K. Kumar, C.-J. Sung, An experimental study of the autoignition characteristics of conventional jet fuel/oxidizer mixtures: Jet-A and JP-8, Combust. Flame 157 (2010) 676–685.
[56] D.A. Rothamer, L. Murphy, Systematic study of ignition delay for jet fuels and diesel fuel in a heavy-duty diesel engine, Proc. Combust. Inst. 34 (2013) 3021–3029.
[57] K.E. Far, F. Parsinejad, H. Metghalchi, Flame structure and laminar burning speeds of JP-8/air premixed mixtures at high temperatures and pressures, Fuel 89 (2010) 1041–1049.
[58] C. Wu, C.K. Law, On the determination of laminar flame speeds from stretched flames, Symp. (Int.) Combust. 20 (1985) 1941–1949.
[59] K. Kumar, C.-J. Sung, X. Hui, Laminar flame speeds and extinction limits of conventional and alternative jet fuels, Fuel 90 (2011) 1004–1011.
[60] X. Hui, C.-J. Sung, Laminar flame speeds of transportation-relevant hydrocarbons and jet fuels at elevated temperatures and pressures, Fuel 109 (2013) 191–200.
[61] S. Humer, A. Frassoldati, S. Granata, T. Faravelli, E. Ranzi, R. Seiser, K. Seshadri, Experimental and kinetic modeling study of combustion of JP-8, its surrogates and reference components in laminar nonpremixed flows, Proc. Combust. Inst. 31 (2007) 393–400.
[62] K. Seshadri, S. Humer, R. Seiser, Activation-energy asymptotic theory of autoignition of condensed hydrocarbon fuels in non-premixed flows with comparison to experiment, Combust. Theor. Model. 12 (2008) 831–855.
[63] S. Humer, R. Seiser, K. Seshadri, Experimental investigation of combustion of jet fuels and surrogates in nonpremixed flows, J. Propul. Power 27 (2011) 847.
[64] R.K. Gehmlich, A. Kuo, K. Seshadri, Experimental investigations of the influence of pressure on critical extinction conditions of laminar nonpremixed flames burning condensed hydrocarbon fuels, jet fuels, and surrogates, Proc. Combust. Inst. 35 (2015) 937–943.
[65] B. Li, N. Liu, R. Zhao, F.N. Egolfopoulos, H. Zhang, Extinction studies of flames of heavy neat hydrocarbons and practical fuels, J. Propul. Power 29 (2013) 352–361.
[66] C. Liu, Z. Li, H. Wang, Drag force and transport property of a small cylinder in free molecule flow: a gas-kinetic theory analysis, Phys. Rev. E 94 (2016) 023102.
[67] C. Liu, W.S. McGivern, J.A. Manion, H. Wang, Theory and experiment of binary diffusion coefficient of *n*-alkanes in dilute gases, J. Phys. Chem. A 120 (2016) 8065–8074.
[68] C. Liu, R. Zhao, R. Xu, F.N. Egolfopoulos, H. Wang, Binary diffusion coefficients and non-premixed flames extinction of long-chain alkanes, Proc. Combust. Inst. 36 (2017) 1523–1530.
[69] E. Ranzi, T. Faravelli, P. Gaffuri, A. Sogaro, Low-temperature combustion: automatic generation of primary oxidation reactions and lumping procedures, Combust. Flame 102 (1995) 179–192.
[70] A. Stagni, A. Cuoci, A. Frassoldati, T. Faravelli, E. Ranzi, Lumping and reduction of detailed kinetic schemes: an effective coupling, Ind. Eng. Chem. Res. 53 (2013) 9004–9016.
[71] L. Esclapez, P.C. Ma, E. Mayhew, R. Xu, S. Stouffer, T. Lee, H. Wang, M. Ihme, Fuel effects on lean blow-out in a realistic gas turbine combustor, Combust. Flame 181 (2017) 82–99.
[72] A. Felden, L. Esclapez, E. Riber, B. Cuenot, H. Wang, Including real fuel chemistry in large-Eddy simulations, Combust. Flame (2018). in press.